A&A 562, A28 (2014)
DOI: 10.1051/0004-6361/201322545

Astronomy & Astrophysics

The spectroscopic evolution of the recurrent nova T Pyxidis during its 2011 outburst

III. The ultraviolet development from iron curtain through the post-X-ray turnoff⋆,⋆⋆

I. De Gennaro Aquino[1], S. N. Shore[1,2,3], G. J. Schwarz[4], E. Mason[5], S. Starrfield[6], and E. M. Sion[7]

[1] Dipartimento di Fisica "Enrico Fermi", Università di Pisa; Largo Pontecorvo 3, 56127 Pisa, Italy
e-mail: ivan.degennaroaquino@gmail.com; shore@df.unipi.it
[2] INFN- Sezione Pisa, largo B. Pontecorvo 3, 56127 Pisa, Italy
[3] Astronomicky Ustav UK., V Holesovickach 2,180 00 Praha 8, Czech Republic
[4] American Astronomical Society, 2000 Florida Ave NW, Washington DC 20009-1231, USA
e-mail: greg.schwarz@aas.org
[5] INAF – Osservatorio Astronomico di Trieste, 34 143 Trieste, Italy
[6] School of Earth and Space Exploration, Arizona State University, PO Box 871404, Tempe, AZ 85287-1404, USA
e-mail: sumner.starrfield@asu.edu
[7] Department of Astronomy and Astrophysics, Villanova University, 800 Lancaster Avenue, Villanova, PA 19085, USA
e-mail: edward.sion@villanova.edu

Received 26 August 2013 / Accepted 13 November 2013

ABSTRACT

We continue the analysis of the multiwavelength evolution of the recurrent nova T Pyx during its 2011 outburst, focussing on the spectral development on the 1150–3000 Å region. This extraordinary data set presents the longest temporal baseline high resolution view of the ultraviolet for any nova to date (classical or recurrent). The observations cover the early Fe-curtain stage, when the UV was completely optically thick, to 834 days after discovery when the outburst was effectively over. We present an analysis of dynamics and abundances of the interstellar species whose resonance lines are accessible in the UV. The Lyα profile is consistent with only interstellar absorption at all epochs and agrees with the H I 21 cm column density. The distance obtained to T Pyx is about 5 kpc, based on the ISM analysis. For the ejecta evolution we have been able to follow the changes in ionization and structure with previously unobtained resolution and cadence. The excited state isoelectronic transitions of C III, N IV], and O V displayed the same detached absorption lines as the optical He I transitions during the optical maximum. This is explained as resonance absorption within the ejecta of FUV ground state lines from the 300–1000 Å range. The resonance lines of all species showed absorption components between –1000 and –3000 km s^{-1} as soon as the Fe-curtain turned transparent (from day 105); these persisted at the same velocities and varied in strength from one ion to another through day 834. The last ultraviolet spectrum, taken more than 800 days after outburst, showed the same absorption lines on N V and C IV as day 105. There was no evidence of circumstellar absorbers. This and the related observations of profile evolution effectively rule out any wind model for the spectrum. The picture that emerges is of ejecta that became optically thin after visual maximum as the X-ray emission became visible following an outwardly propagating ionization front and for which the ionization stages froze because of ejecta expansion after the end of the soft X-ray illumination.

Key words. novae, cataclysmic variables – line: profiles – stars: individual: T Pyx – ultraviolet: stars – circumstellar matter

1. Introduction

The sixth outburst of the recurrent nova T Pyxidis was detected on 2011 Apr. 14.2931 (MJD 55665.79310, hereafter taken as our reference date for time since outburst) by Wagan et al. (2011). Panchromatic observations were obtained contemporaneously with groundbased telescopes and space instruments. Shore et al. (2011, hereafter Paper I) presented the analysis of optical high resolution spectra taken during the optically thick phase of the outburst, while late stage transition to nebular phase was discussed in Shore et al. 2012 (hereafter Paper II). We proposed a new explanation for the moving lines phenomenon, typical of the optically thick stage when P Cyg profiles show fragmented structures, and the bipolar geometry of the ejecta, confirmed by radio and optical interferometric observations (Nelson et al. 2013; Chesneau et al. 2011). Important aspects remain, however, mysterious, e.g. the prolonged visual maximum phase, the peculiar profiles from high ionization species, and the fine structure of the ejecta.

Two long observing programs with the *Hubble* Space Telescope in Cycles 18 and 19 were activated to investigate the nova and supplemented with Director's Discretionary time for this extraordinary event. High and medium resolution echelle

⋆ Based on observations made with the NASA/ESA *Hubble* Space Telescope, obtained from the data archive at the Space Telescope Science Institute. STScI is operated by the Association of Universities for Research in Astronomy, Inc. under NASA contract NAS 5-26555.

⋆⋆ Based on observations made with the Nordic Optical Telescope, operated on the island of La Palma jointly by Denmark, Finland, Iceland, Norway, and Sweden, in the Spanish Observatorio del Roque de los Muchachos of the Instituto de Astrofisica de Canarias.

Table 1. Journal of STIS observations.

STIS OBSID	JD 2 450 000+	t_{exp} (s)	Grating
2011 May 06 (day 23)			
OBG101010	5688.335	571	E140M
OBG101020	5688.345	571	E230M
OBG101030	5688.356	571	E230H
2011 Jul. 28 (day 105)			
OBG199010	5770.786	285	E140M
OBG199020	5770.794	285	E230M
OBG199030	5770.801	35	E230H
OBG199040	5770.805	1	G430M
PBG199050	5770.810	1	G430M
OBG199060	5770.814	1	G750M
2011 Oct. 04 (day 173)			
OBG103010	5838.540	600	E140M
OBG103020	5838.552	600	E230M
OBG103040	5838.567	155	E230M
OBG103030	5838.561	5	G430L
2012 Mar. 28 (day 349)			
OBX701010	6014.643	2457	E140M
OBX701020	6014.702	3023	E140M
2012 Dec. 21 (day 617)			
OBXS01010	6282.221	2449	E140M
OBXS01020	6282.279	3015	E140M
2013 Jul. 26 (day 834)			
OBXS03010	6499.875	2449	E140M
OBXS03020	6499.917	3015	E140M

spectra obtained from 2011 May 2011 to 2013 July cover the ultraviolet spectroscopic evolution of the outburst from optical maximum through the post-X-ray emission stage. This is a unique sample, providing a view of the outburst not heretofore possible for any other classical or recurrent nova.

For novae, the presence in late time spectra of absorption features related to the ejecta has been reported by Cassatella et al. (2004). As we will discuss here, T Pyx also showed this behavior. The outburst provides an opportunity to determine the properties of the interstellar medium (ISM) toward the nova, a line of sight that has not been well sampled in the Galaxy. The identification of ISM lines is ideally an easier task due to their small, constant radial velocity range and obvious persistence across all the observations, while the ejecta features are strongly correlated with the density and ionization conditions in which they are formed, thus changing and evolving like the emission lines.

In the following sections, we first discuss the results for the ISM along the line of sight to T Pyx, its velocity structure and column densities, and their implications for the distance, extinction, and intrinsic properties of the nova. We then present the development of the ultraviolet spectrum of the nova ejecta.

2. Observational data

We used ultraviolet spectra obtained with the Space Telescope Imaging Spectrograph (STIS) aboard the *Hubble* Space Telescope. These were supplemented with optical spectra obtained with the fiber-optic echelle spectrograph (FIES) at the 2.6 m Nordic Optical Telescope (NOT) described in Paper II. The complete journal of the observations is reported in Table 1. Ultraviolet mid-resolution spectra covered the fully available wavelength range for STIS, from 1150 Å to 3100 Å, only for the first three epochs (GO 12200), while epoch 4 through 6 (GO 12799) observations only used the E140M grating spectrum (1150 Å to 1700 Å). For the visual spectral range, we used NOT spectra from Papers I and II, and data obtained during the 2011 Jul. 28 visit that included three optical spectra obtained with the G430M and G750M gratings in limited wavelength intervals and one with the G430L on 2011 Oct. 4. All exposures were taken with the 0.2×0.2 arcsec^2 aperture.

Our high resolution NOT spectra (see Papers I and II) were supplemented with two X-Shooter VIS arm spectra obtained on 2011 June 21 and 26 (days 68 and 73) to monitor the evolution of the HeI 5876 Å line. These cover the wavelength range ~5500–10 200 Å at a resolution $R \approx 18\,000$ for the adopted slit of 0.4 arcsec. The spectra were downloaded from the ESO archive and reduced with the *esorex* pipeline version 1.2.2.

3. Interstellar absorption lines

In Paper I, the interstellar optical absorption along the line of sight to T Pyx spectra were shown to coincide with the radial velocities of the H I 21 cm emission in the GASS spectrum (Kalberla et al. 2010). The UV interstellar lines show the same agreement. Figures 1–3 show a selection of interstellar lines: the first figure includes optically thin transitions and 21cm neutral hydrogen emission, saturated lines and high ionization species in the following figures. Each profile was selected from the epoch that presented the highest signal-to-noise ratio in the specific wavelength range for its transition. In Table 2 we list the identified lines and, where measured, their equivalent widths.

Before proceeding, a word about methodology. These data may not seem ideal for ISM investigation. The interstellar absorption lines are formed against a non-stationary source, with a spectrum strongly variable between the epochs, changing in both continuum and lines emission fluxes. In fact, many lines were visible only because of strong (line) emission in those specific wavelength intervals. But the variability of the underlying spectrum actually aids in their identification since the ISM lines are the only permanent features throughout the outburst.

Several species displayed optically thin profiles: Al II, C I, Cl I, Cr II, Fe II, Mg I/II, Mn II, N I, Ni II, Si II, and Zn II. These transitions all show a similar profile, with a mean radial velocity in agreement with the 21 cm emission core. A few lines, e.g. Cl I 1347.24 Å and the Mg II 1240 Å doublet, were sufficiently resolved to show two distinct components at $v_{LSR} = +11$ km s^{-1} and +22 km s^{-1}. The molecular transition ^{12}CO A-X(3,0) at 1447.335 Å was only measurable in the day 23 spectrum; its velocity agreed with the other optically thin ISM features. A number of saturated lines originated from low ionization strong transitions: C II, Mg I/II, O I, S II, Si II. The profiles were completely opaque in the core and wings extend from −30 to +100 km s^{-1}, covering the same velocity range spanned by the 21 cm spectrum. More highly ionized species were also present: Al III, C IV, Si III/IV. These ions showed profiles that, although not completely saturated, were broad, extending from –10 to +80 km s^{-1}. Si III lines suffered from very low signal-to-noise ratio and its greater velocity width is probably caused by noise.

For low ionization species (Cl I, Cr II, Fe II, Mg II, Mn II, N I, Ni II, S II, Si II, Zn II) we assembled a curve of growth with a single Gaussian component to estimate the column density. This approximation assumes that a single cloud is responsible for the absorption spectrum, which contrasts with the observational evidence of at least two components for many optically thin lines observed. This technique also reduces all the information on the

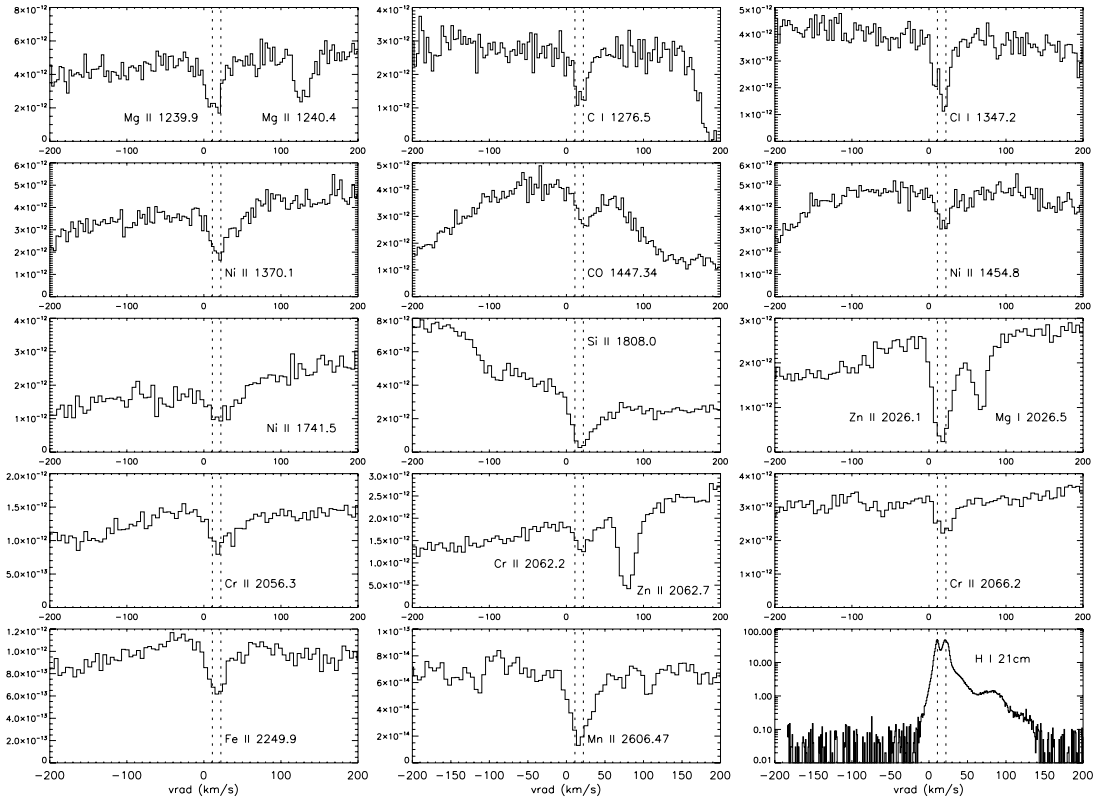

Fig. 1. Gallery of the UV interstellar lines observed with HST/STIS and 21cm neutral hydrogen line profile from the GASS survey. All velocities are *heliocentric*. On *y*-axis: flux (erg s^{-1} cm^{-2} Å^{-1}), temperature (K) for the 21cm profile. Dotted lines mark +11 and +22 km s^{-1} radial velocity. These first panels show the optically thin line (no smoothing applied).

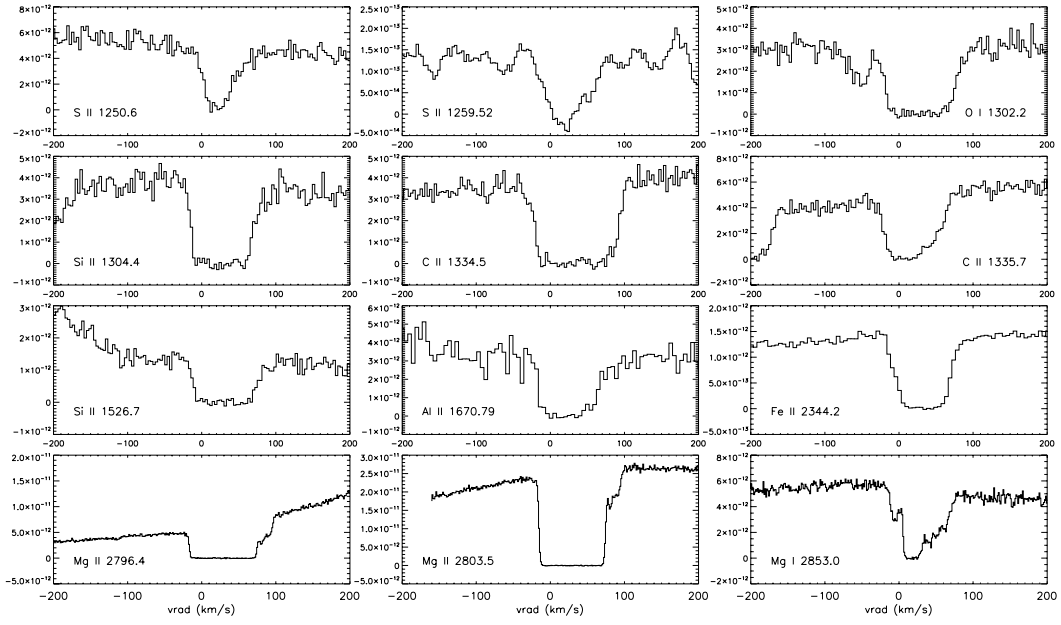

Fig. 2. As in Fig. 1, displaying the saturated interstellar lines (no smoothing applied).

velocity span of the interstellar line in one single velocity spread parameter *b*. However, Jenkins (1986) suggests that the estimate of column densities with a single Gaussian component curve of growth does not dramatically differ from a detailed profile fitting technique, with the difference being less or comparable to the observational error in case of poorly resolved lines. The equivalent width measurements are plotted in Fig. 4 with the theoretical curve of growth used to derive the column densities reported in Table 2. The best-fit value obtained for the velocity spread parameter *b* is 18.8 ± 0.2 km s^{-1}, with χ^2/(d.o.f.) = 1.28.

High ionization species, Al III, C IV and Si IV, showed profiles with enhanced optical depth on the positive velocity wing with respect to the central velocity. For these lines, characterized by unsaturated profiles, we estimate the column densities with:

$$N = \frac{m_e c^2}{\pi e^2 f \lambda^2} W_\lambda[\text{mÅ}] = 1.13 \times 10^{17} \frac{W_\lambda[\text{mÅ}]}{f \lambda^2[\text{Å}]} \quad (1)$$

Table 2. Ultraviolet ISM lines.

Species	Obs	λ^a (Å)	f^b	EW (mÅ)	Note
Si II	3	1190.42	0.277	350 ± 30	(s)
Si II	3	1193.29	0.575	410 ± 50	(s)
N I	3	1199.55	0.132	380 ± 50	(s)
N I	3	1200.22	0.0869	330 ± 50	(s)
N I	3	1220.71	0.0432	300 ± 50	(s)
Si III	3	1206.51	1.67	500 ± 60	(s)
Mg II	2	1239.93	6.21e-4	68 ± 8	
Mg II	2	1240.40	3.51e-4	55 ± 7	
S II	1	1250.58	6.02e-3	205 ± 18	
S II	1	1253.81	0.0121	235 ± 25	(s)
S II	1	1259.52	0.0182	320 ± 30	(s)
Si II	2	1260.42	1.22	–	(s); bl. C I 1260.74 Å
C I	2	1276.48	3.69e-3	49 ± 8	
C I	2	1277.25	–	–	bl. C I 1277.53 Å
C I	2	1280.135	0.0261	105 ± 13	
P II	2	1301.87	0.038	$\gtrsim$70 ± 10	
O I	2	1302.17	0.052	440 ± 20	(s)
Si II	2	1304.37	0.0928	363 ± 16	(s)
Ni II[c]	2	1317.22	0.0571	56 ± 13	
C I	3	1328.834	0.058	190 ± 20	
C I	3	1329.1	–	–	unresolved triplet
C I	3	1329.6	–	–	unresolved doublet
C II	1	1334.53	0.129	508 ± 15	(s)
C II	1	1335.71	0.115	318 ± 19	(s)
Cl I	2	1347.24	0.114	53 ± 5	
Ni II[c]	2	1370.13	0.0588	70 ± 9	
Si IV	2	1402.77	0.255	38 ± 12	
^{12}CO[d]	1	1447.335	0.0361	43 ± 7	
Ni II[c]	1	1454.84	0.026	22 ± 5	
Si II	1	1526.72	0.133	468 ± 45	(s)
C IV	2	1548.20	0.190	159 ± 20	
C IV	2	1550.77	0.0952	67 ± 10	
C I	2	1560.31	0.0716	208 ± 15	
C I	2	1560.7	–	–	unresolved doublet
Fe II	1	1608.45	0.0591	320 ± 20	
C I	2	1656.267	0.0598	97 ± 15	
C I	2	1656.928	0.143	–	(s); bl. C I 1657.01 Å
C I	2	1657.379	0.0357	59 ± 15	
C I	2	1657.907	0.0476	70 ± 15	
Al II	2	1670.79	1.83	443 ± 28	(s)
Ni II[c]	2	1741.55	0.0427	70 ± 12	
Ni II[c]	2	1751.91	0.028	57 ± 10	
Si II	1	1808.01	2.49e-3	240 ± 30	
Al III	1	1854.72	0.557	194 ± 17	
Al III	1	1862.79	0.277	111 ± 9	
Zn II	1	2026.14	0.515	180 ± 15	
Mg I	1	2026.48	0.113	$\gtrsim$115 ± 10	
Cr II	1	2056.25	0.105	103 ± 8	
Cr II	1	2062.23	0.078	72 ± 6	
Zn II	1	2062.66	0.2529	154 ± 15	
Cr II	1	2066.16	0.0515	52 ± 5	
Fe II	1	2249.88	1.82e-3	65 ± 15	
Fe II	1	2260.78	2.44e-3	122 ± 13	
Fe II	1	2344.21	0.114	607 ± 24	(s)
Fe II	3	2374.46	0.0359	497 ± 37	
Fe II	3	2382.76	0.320	717 ± 48	(s)
Mn II	3	2576.88	0.3610	418 ± 35	
Fe II	3	2586.65	0.0717	597 ± 50	(s)
Mn II	3	2594.51	0.28	406 ± 26	
Fe II	3	2600.17	0.239	763 ± 53	(s)
Mn II	3	2606.47	0.198	228 ± 32	
Mg II	1	2796.35	0.608	976 ± 23	(s)
Mg II	1	2803.53	0.303	895 ± 22	(s)
Mg I	1	2852.96	1.800	550 ± 25	(s)

Notes. [(a)] Laboratory vacuum wavelengths. [(b)] All f-values from Morton (2003), unless otherwise indicated. [(c)] f-values from Jenkins et al. (2006). [(d)] f-value from Welty et al. (1992). (s) Indicates saturated profile.

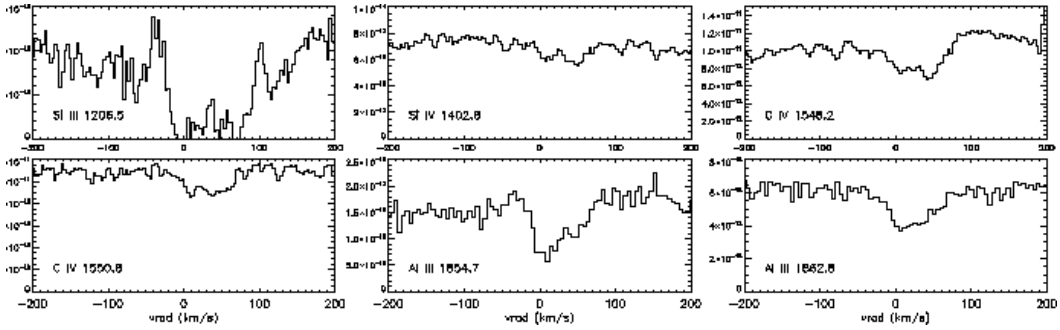

Fig. 3. As in Fig. 1, displaying the high ionization species interstellar lines (3 point boxcar smoothing applied).

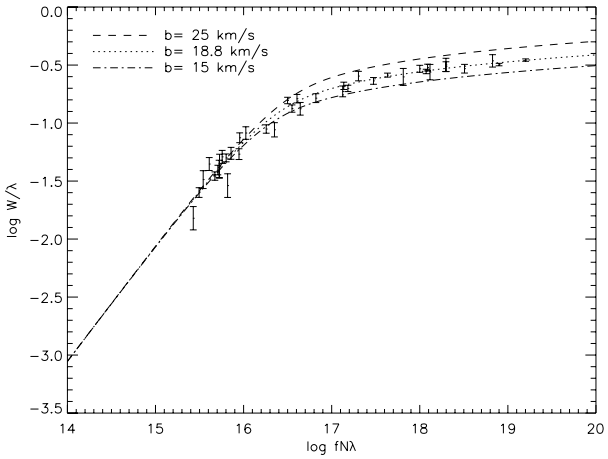

Fig. 4. Curve of growth for low ionization species. The best fit model curve has $b = 18.8$ km s^{-1}, with χ^2/(d.o.f.) ~ 1.28.

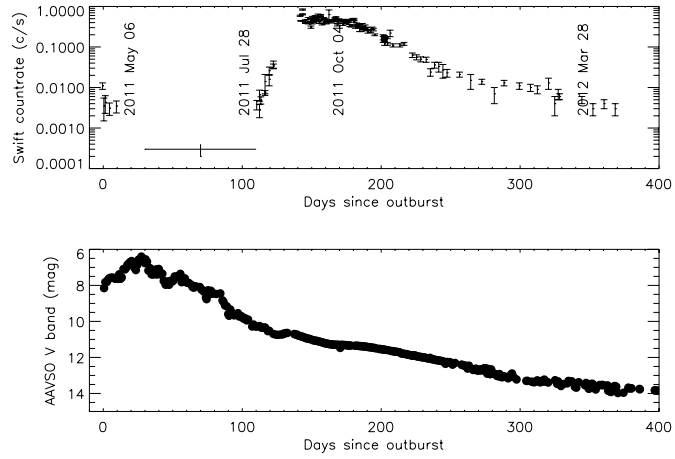

Fig. 5. *Top*: X-ray light curve from *Swift*/XRT (0.3–10 keV) until day 400 of the 2011 outburst. The first four STIS observations are marked (see Table 1). *Bottom*: daily averaged AAVSO visual light curve through the outburst.

since the number of lines is not sufficient to form a combined curve of growth. We used the same equation to derive a lower limit on the column densities for saturated lines or blended transitions for which we have only a lower limit on the equivalent width (Al II, C II, Mg I, O I, P II, Si III). The presence of these high ionization absorptions extending to high positive velocity (~+60 km s^{-1}) clearly shows the presence of warm gas along the line of sight.

Finally, on the question of the distance to T Pyx, we use an example based on the Mg II 2800 Å doublet (Fig. 2). The high signal-to-noise ratio for the day 23 spectrum with the E230H grating shows that the doublet lines were completely opaque from –10 to 70 km s^{-1} with unsaturated components clearly present at ~+80 km s^{-1}. Using the third quadrant Galactic rotation curve (Brand & Blitz 1993) we find a distance to T Pyx of ≈5 kpc based on the presence of this high radial velocity component. Lines of other species, shown in Figs. 2 and 3, also show this high velocity component.

Table 3. Column densities derived with the curve of growth displayed in Fig. 4.

Species	-1σ	Log N (cm^{-2})	$+1\sigma$
H I[a]	21.40	21.48	21.54
Al II		>12.99	
Al III	13.03	13.09	13.14
C I	14.43	14.50	14.57
C II		>14.40	
C IV	13.47	13.56	13.64
Cl I	13.47	13.52	13.57
Cr II	13.42	13.47	13.51
Fe II	15.03	15.21	15.39
Mg I		>13.44	
Mg II	15.86	15.97	16.07
Mn II	13.55	13.64	13.73
N I	15.61	16.10	16.68
Ni II	13.75	13.85	13.94
O I		>14.75	
P II		>14.09	
S II	15.75	15.94	16.17
Si II	15.61	15.98	16.40
Si III		>13.37	
Si IV	12.76	12.93	13.05
Zn II	13.18	13.24	13.29
^{12}CO	13.73	13.81	13.87

Notes. [(a)] Hydrogen column density as derived in Paper II. [(b)] Column densities estimated with Eq. (1). Asterisks indicate column densities for excited states.

4. Ejecta evolution

We first comment on the global picture provided by the full ultraviolet range before going into details regarding the individual diagnostics of the ejecta structure and dynamics. Of the novae that have been observed at high resolution in the ultraviolet with either the GHRS or STIS, V1974 Cyg, V382 Vel, LMC 2000, and V959 Mon (all ONe types, see, e.g. Shore et al. 2013) none was a recurrent nova[1] and no nova has previously been observed at the same resolution at a time later than about 200 days after outburst. With T Pyx we enter new territory. For reference

[1] The only high resolution spectra for U Sco 1999 in outburst were an N III] 1750 Å spectrum and an Hα observation, both taken with STIS.

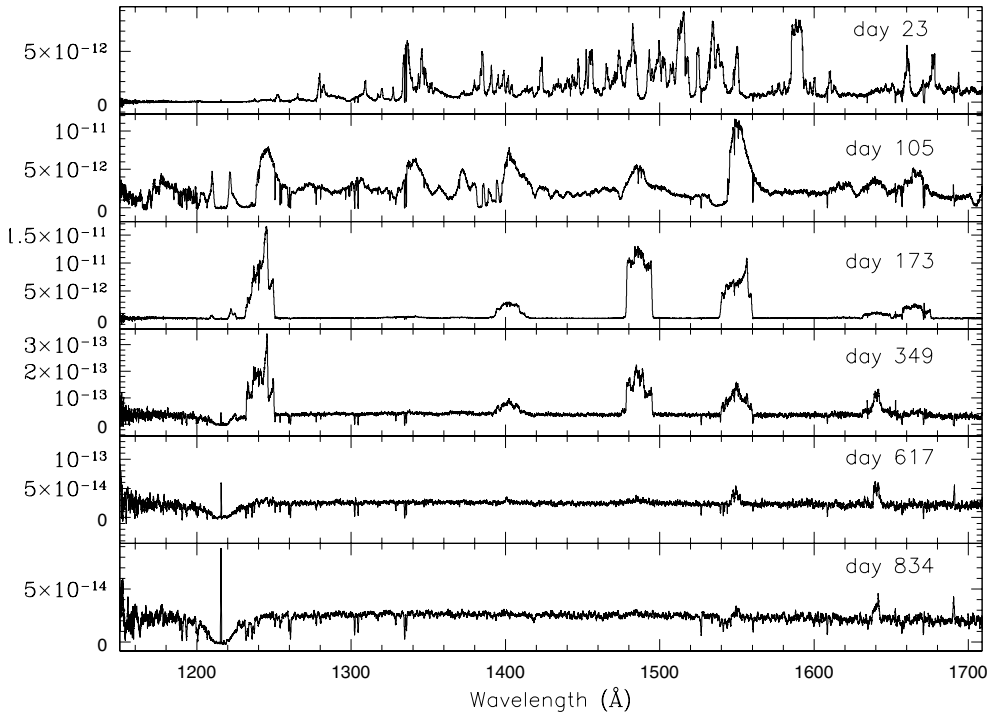

Fig. 6. UV spectra with the E140M grating showing the continuum from 1200–1700 Å from the STIS observations. *From top*: day 23 (optical maximum, boxcar smoothed by 7 points), 105 (start of SSS emission, smoothed by 11 points), 173 (peak of SSS phase, smoothed by 7 points), 349 (end of SSS phase, smoothed by 15 points), 617 (smoothed by 21 points), and 834 (post-SSS, smoothed by 33 points). The last three dates did not include spectra longward of 1700 Å. See text for details. All fluxes are uncorrected absolute values, erg s^{-1} cm^{-2} Å^{-1}.

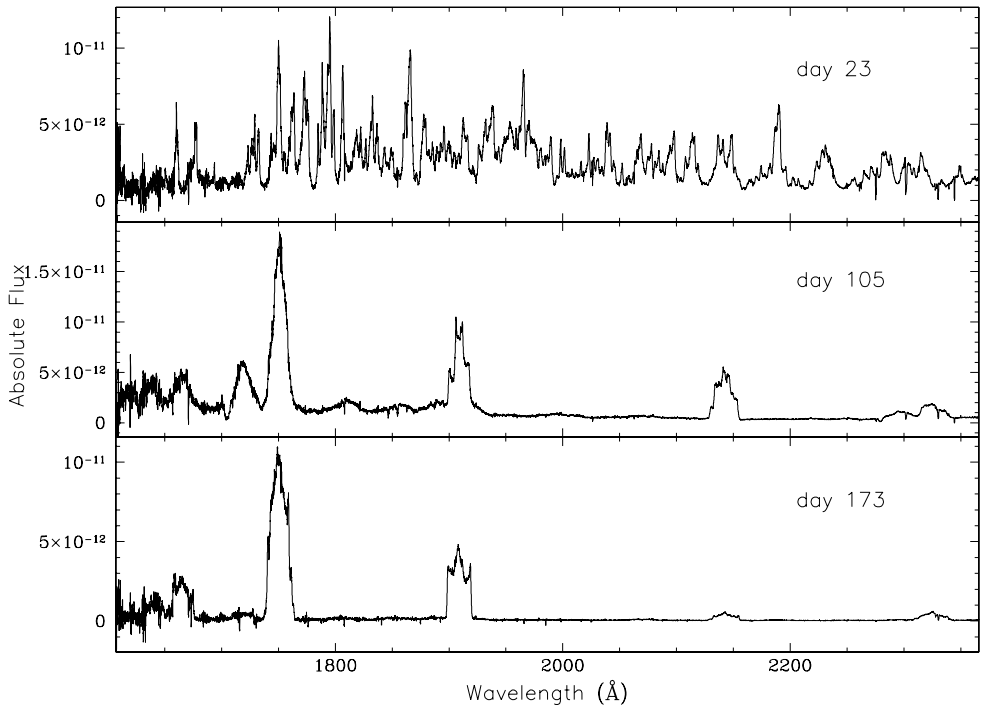

Fig. 7. Same as Fig. 6, UV spectra with the E230M grating.

in our discussions, we show in Fig. 5 the optical and X-ray light curves with the times of our HST/STIS observations indicated. Days 617 and 834, were obtained after the end of the *Swift* campaign. The HST/STIS coverage of the outburst began early enough that the first spectra, on day 23, were during the Fe-curtain phase and this is evident from the first sequence of spectra shown in Figs. 6 through 8.

4.1. Day 23: the Fe-curtain stage and luminosity estimate

In the first spectrum, obtained on day 23, only pseudo-emission peaks were present from the usual windows among the bands of heavy metal absorption systems. It is important to note that these are the same transitions that produce the optical Fe-peak emission typical of the so-called Fe-nova stage (e.g. Williams 1991, 1994; Shore 2008). The velocity range of the ejecta was sufficiently large that the bands are merged and the individual narrow absorption lines that are evident on the optical transitions at the same stage (Paper I) cannot be distinguished. There was a hint of a few nascent emission lines, all from neutral (O I 1302 Å) and singly ionized (C II 1334 Å and N II 2145 Å) beneath the curtain as indicated by their later appearance in the same velocity interval. The one strong emission feature was the Mg II h and k doublet which appeared to display a P Cyg absorption trough extending to –2000 km s^{-1}. This is the same as

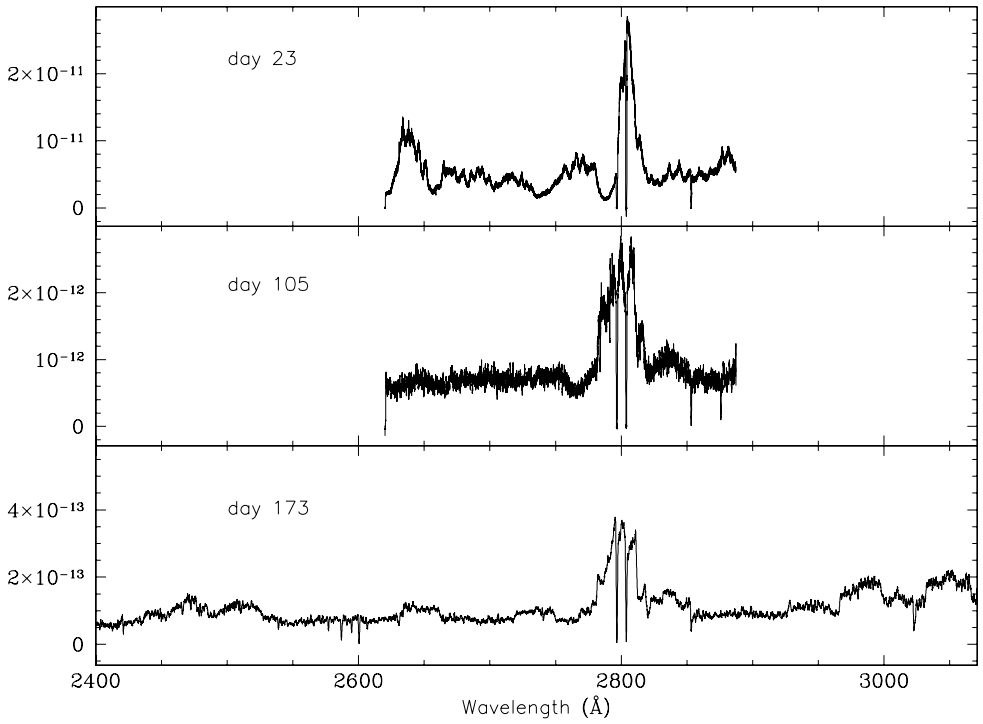

Fig. 8. Same as Fig. 6, UV spectra including the Mg II doublet with the E230H (days 23 and 105) and E230M (day 173) gratings.

the extent of the blue emission wing and the HWZI of the later emission profile.

An important feature of this spectrum is that the residual intensity was not zero for the ejecta, as shown by the visibility of the interstellar absorption lines discussed in the previous section. The minimum flux (not dereddened) was $\approx 5 \times 10^{-13}$ erg s^{-1} cm^{-2} Å^{-1} throughout the 1200–2900 Å range. That this cannot be an instrumental effect is demonstrated by the saturated ISM lines, especially the C II 1334 Å and Mg II 2800 Å doublets; it is the combined effect of velocity desaturation and possible porosity of the ejecta. The luminosity of any nova is a fundamental, but hard to measure, property. The shift in the continuum peak to unmeasurable far ultraviolet bands occurs early in the event once the Fe-curtain becomes transparent. It is possible, however, to obtain some limits if the panchromatic continuum is available during the optically thick stage. Fortunately, the first STIS observation was during optical maximum and at around the same time as a NOT optical spectrum (on day 33) for which a spectrophotometric standard star was observed (see Paper II). The MMRD relation (Della Valle & Livio 1995) provides a rough estimate of $M_V = -7.3 = 5.0 \times 10^4\ L_\odot$ in the visible alone, using $t_2 = 32$ days (Schafer 2010). The combined ultraviolet and optical spectra, although containing some gaps in coverage, yield a measured flux of $(3.2 \pm 0.2) \times 10^{-8}$ erg s^{-1} cm^{-2} in the interval from 1200–7300 Å which becomes $(3.2 \pm 0.2) \times 10^{-7}$ erg s^{-1} cm^{-2} when corrected using $E(B-V) = 0.5$ (using Cardelli et al. 1989, see Paper I). The systematic uncertainty in the optical calibration was about 30%, mainly below 4000 Å and 20% longward. For a reference distance of 5 kpc, this flux corresponds to an *uncorrected* luminosity of $\geq 2.5 \times 10^4\ L_\odot$. With the reddening correction, this becomes $2.5 \times 10^5\ L_\odot$. The value is very large but this is actually a lower limit on the total luminosity at this stage – for this choice of extinction and distance – since the ejecta are not spherically symmetric. Several novae have reached such large values above the Eddington limit, e.g., nova LMC 1991 for which the distance is known (Schwarz et al. 2001). For any extinction and distance previously published in the literature (see Paper I) this value implies a massive WD, near the Chandrasekhar limit, For instance, the *minimum* luminosity, corresponding to $E(B-V) = 0.3$ (e.g. Selvelli et al. 2008; Schaefer et al. 2013) and a distance of 3.5 kpc, is $4.5 \times 10^4\ L_\odot$. Even this luminosity implies a higher mass than inferred from the orbital solution (Uthas et al. 2010). Note, however, that the red dwarf can also be more massive since only the mass ratio was obtained from the radial velocity analysis. The distance of 4.8 kpc implied by the light echo (Sokoloski et al. 2013) is about the same as our proposed distance while the 3.5 kpc distance (Selvelli et al. 2008) is at the lower limit possible from the interstellar profiles and the MMRD relation seems to fail for T Pyx.

4.2. Day 105: emergence of X-ray emission

The second observation, on day 105, was after the end of the Fe-curtain stage and at the start of brightening in the X-rays as observed by *Swift* (Kuulkers et al. 2011). The X-ray flux was about 1% of its eventual peak intensity at this stage (see Fig. 5). Continuum emission was detected throughout the UV range against which the strong transitions showed P Cyg absorption troughs. The nova had by this epoch entered the transition stage, defined by the onset of intercombination and forbidden line emission. The observed emission lines included: C III 1175, N V 1240, O I 1302, C II 1334, O V] 1371, Si IV/O IV 1400, N IV] 1486, C IV 1550, He II 1640, O III] 1667, N IV] 1718, N III] 1751, Si II 1810, Al III 1860, C III] 1909, N II] 2145, C III 2296, C II] 2324, and Mg II 2800 Å.

4.3. Day 173: nebular phase and peak of the soft X-ray emission

The third spectrum, from day 173, was obtained near the observed peak of the soft X-ray emission. The continuum was considerably weaker and the absorption troughs were absent even for the strongest resonance lines. The profiles were, however, systematically asymmetric, a point to which we will re-

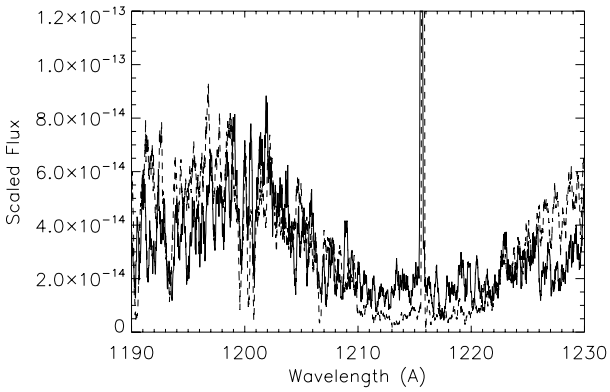

Fig. 9. Comparison of the Lyα line from the day 23 (solid) and day 617 (dash) spectra. The latter was scaled by a factor of 3 in continuum flux for epoch. Note the invariance of the wings of the profile, consistent with only an interstellar contribution throughout the UV spectral sequence. The emission spike is geocoronal Lyα.

turn presently. The days 173 and 349 spectra were discussed in Paper II. We note that at no stage after the end of the Fe-curtain did T Pyx ever display any Ne ion lines. This spectrum, and the next from the day 349, compared with Figs. A.1 and A.2 of Shore et al. (2013b) for the ONe novae, demonstrates that *the WD in the T Pyx system is not of the oxygen-neon type*.

4.4. Day 349: end of the X-ray phase

Starting with the day 349 observation, only the range shortward of 1700 Å was observed. The day 349 spectrum was obtained at the end of the SSS stage and showed a substantially weaker continuum, no P Cyg lines, and only emission from the strongest resonance transitions. By this stage, the O I 1302 Å line had vanished and the 1400 Å feature was likely produced by O IV 1402 Å, not Si IV 1400 Å, as noted in other high resolution studies (see Shore et al. 2013b).

4.5. Days 617 and 834: post-outburst

Two epochs were observed after the end of the X-ray emission and in the late decline stage of the outburst. The first, on day 617, showed a featureless continuum with weak emission from only C IV 1550 Å and He II 1640 Å. A more complete analysis of the continuum and its implications for the state of the WD in the later stages will appear elsewhere (Sion et al., in prep.). In the day 834 spectrum, aside from the evident continuum emission, the only (weak) emission lines were still C IV 1550 Å and He II 1640 Å with no evidence of any N V emission. The strong Lyα, so evident in this and the previous spectrum, was completely consistent with interstellar absorption alone as shown in Fig. 9.

A sample low resolution *IUE* archival quiescence state observation was retrieved from the MAST, from 1996 May 6 (SWP 57030, LWP 32287), that was about 30 years after the end of the 1966 outburst (see Gilmozzi & Selvelli 2007) that displayed an integrated flux of 2.4×10^{-11} erg s^{-1} cm^{-2}. Applying $E(B-V) = 0.5$, this becomes 1.2×10^{-9} erg s^{-1} cm^{-2}, about 0.3% of the maximum flux we infer from the day 23 data. For comparison, in the day 834 data the continuum level at 1400 Å was 2.8×10^{-14} erg s^{-1} cm^{-2} Å^{-1}, which was nearly the same as in the 1996 spectrum at the same wavelength, 2.3×10^{-14} erg s^{-1} cm^{-2} Å^{-1}, and implies a return to near quiescence.

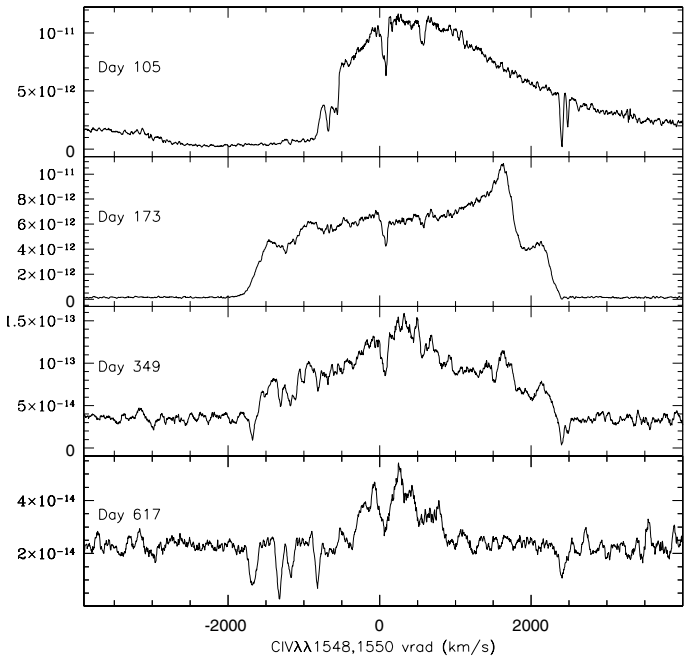

Fig. 10. The C IV 1550 Å doublet profile development. Note the emission feature at +2000 km s^{-1} that indicates the recombination of the receding ejecta at the same velocity as the absorption features that are present in the last spectrum. The narrow lines near $v_{\rm rad} = 0$ are the interstellar C IV absorption lines. All fluxes are uncorrected absolute values, erg s^{-1} cm^{-2} Å^{-1}.

5. Line profile evolution

The analysis of the optical emission line profiles at the same epochs was presented in Paper II. Here we discuss the results obtained from the ultraviolet transitions, which include a wealth of resonance lines of ionization states unobservable at longer wavelengths, and the particular insights they provide. The day 23 spectrum was dominated by the Fe-curtain and the only certain "emission" peaks in the 1200–3000 Å region were windows in the overlying absorption from the optically thick ejecta. At this stage, the optical Fe II lines, and the other strong optical transitions of heavy elements, still displayed absorption components. Note that the lower levels of the strongest optical Fe II transitions, for instance, are directly connected to the ground state through the same multiplets that dominate the curtain. The narrowness of the optical lines, tens of km s^{-1} for the fine structure, shows the fine tuning of the radiative excitation, an effect pointing strongly to the pumping happening in the co-moving frame of the ejecta and not in a wind at terminal velocity, a point to which we will return later.

5.1. Resonance lines: P Cyg profiles

By day 105, the curtain had largely dissipated. The C IV 1550 Å (Fig. 10) and N V 1240 Å resonance doublets (Fig. 11) displayed P Cyg profiles with strong absorption extending to ≈–3200 km s^{-1} and were completely saturated from –1000 to –2500 km s^{-1}. The maximum velocity was greater than any observed in the first optical spectra that were obtained during the fireball stage and before the onset of the recombination wave (see Paper II). The blue edge of the absorption trough is like that observed in the V1974 Cyg (Shore et al. 1994) and V382 Vel (Shore et al. 2003) high resolution spectra. It is not

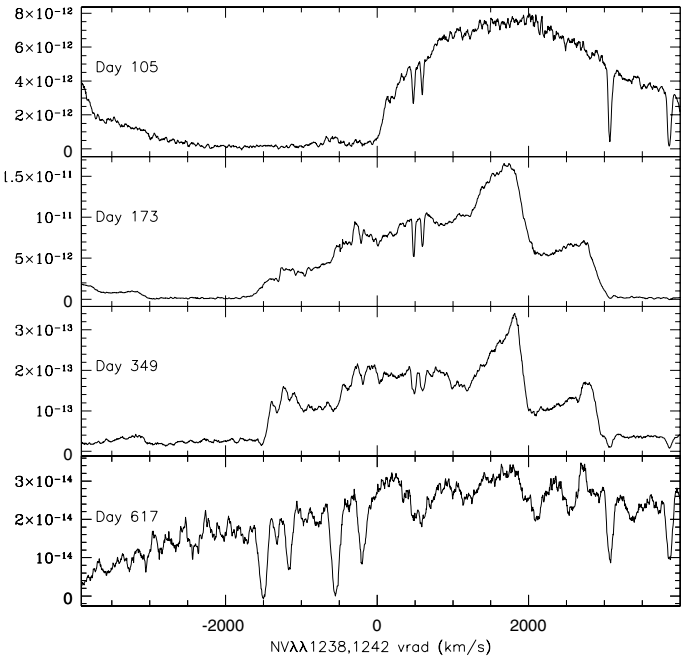

Fig. 11. The N V 1240 Å doublet profile development, as in Fig. 10. Note the presence of the same emission feature at +2000 km s^{-1} as in C IV. The weak narrow lines near $v_{\rm rad}$ = 0 are the interstellar Mg II absorption lines.

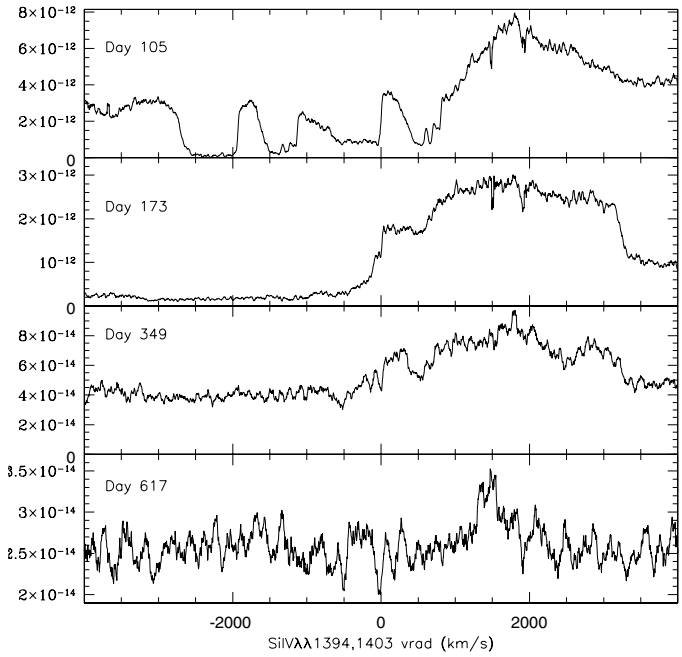

Fig. 12. The Si IV 1400 Å doublet development as in Fig. 10. The emission is a combination of the Si IV and O IV resonance lines, see text for details.

a sharp cutoff, as would be expected for a saturated wind profile even with "turbulence" but instead has a gradual shading to higher velocities that is expected from ejecta (e.g. Hauschildt 2002; Shore 2012). The profiles are not completely opaque even though clearly saturated, as shown by the residual flux at C IV of ~2.3 × 10^{-13} erg s^{-1} cm^{-2} Å^{-1} (uncorrected), slightly lower than on day 23 but not negligible. The N V measurement was complicated by the Lyα wings but had essentially the same line profile.

The Si IV 1400 Å resonance doublet absorption was more complicated (Fig. 12) than the other resonance P Cyg profiles. Instead of showing a uniformly saturated absorption throughout the velocity interval, it displayed a set of broad but distinct absorption features in the intervals –1300 to –1800 km s^{-1} and –1900 to –2300 km s^{-1}. The complexity of the features, analogous to the Na I D lines in the earlier optical NOT spectra up to day 33 discussed in Papers I and II, is illustrated by the difference between the absorption due to the 1396 Å and 1403 Å components of the doublet, see Fig. 13. Similar features were also noted on the Balmer lines in the same period (see Paper I). The visibility of those features was attributed to a recombination wave that moved outward during the initial expansion and cooling of the ejecta and the subsequent increase in the optical depth of the UV ground state transitions of the Fe-group ions. *For Na I, the line formation process is closer to Si IV since it is a resonance line. The same structure was noted on Ca II H and K.* We cannot say whether – as seen earlier for the Na I D lines – the subsequent development would not have been to dissolve in an ensemble of narrower features in the same velocity intervals; we were not able to obtain such high cadence in the observations. Notice that *one* of the pairs of absorption bands in Si IV corresponds to the velocity observed in the optical profile of a neutral species resonance line. The higher velocity component, seen in absorption in both components of the Si IV doublet, had no correspondence for Na I. The difference in time is important: *the same structures,*

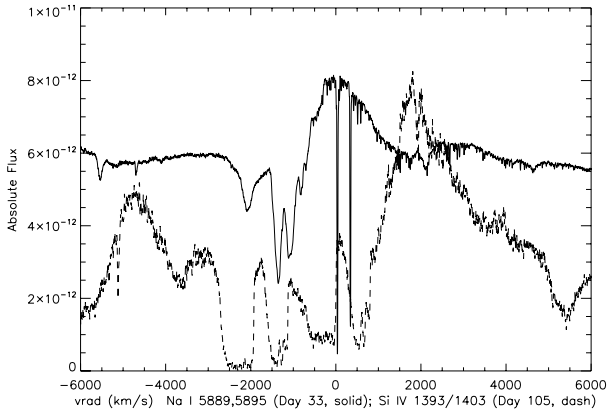

Fig. 13. Comparison of early Na I D line profile at maximum optical brightness (solid) with day 105 Si IV 1393, 1402 Å doublet absorption components (dot). Note that the Na I features at –1300 km s^{-1} were present for both Si IV doublet components while there was no corresponding high velocity feature at –2100 km s^{-1}.

while appearing with different relative strengths in the different ions, were present throughout the event. It seems that the emission at this stage was from the O IV 1402 Å multiplet while the absorption lines were due to the Si IV that was still present in a portion of the ejecta. In Fig. 14, we show the comparison between the Si IV doublet and the Si III 1206 Å resonance line from day 105. The Si III profile was severely blended with interstellar absorption, especially the N I 1199–1201 Å lines, but its disentanglement is assisted by comparing the days 105 and 349 spectra, since only interstellar absorption was seen in the later. Again, the same structures were observed in both ions.

In the day 349 spectrum, there were no longer absorption features on the Si IV 1400 Å and C II 1335 Å doublet components. The emission was also absent (except for a possible very weak emission feature at +2000 km s^{-1}). The C IV and N V resonance doublets were in emission with the asymmetric profiles

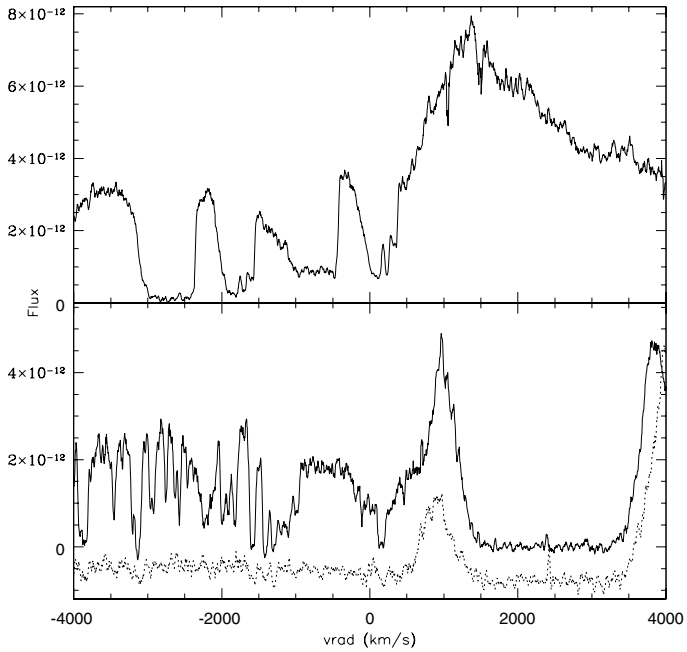

Fig. 14. Comparison of the Si IV doublet (top, day 105) and Si III 1206 Å (bottom, days 105 and 349). The latter has been scaled for the comparison. The only absorption on day 349 was interstellar, mainly Si III 1206 Å and N I 1199–1201 Å. An absorption trough on Si III 1206 Å appears to corresponds to the feature on Si IV at ≈–1500 km s^{-1}.

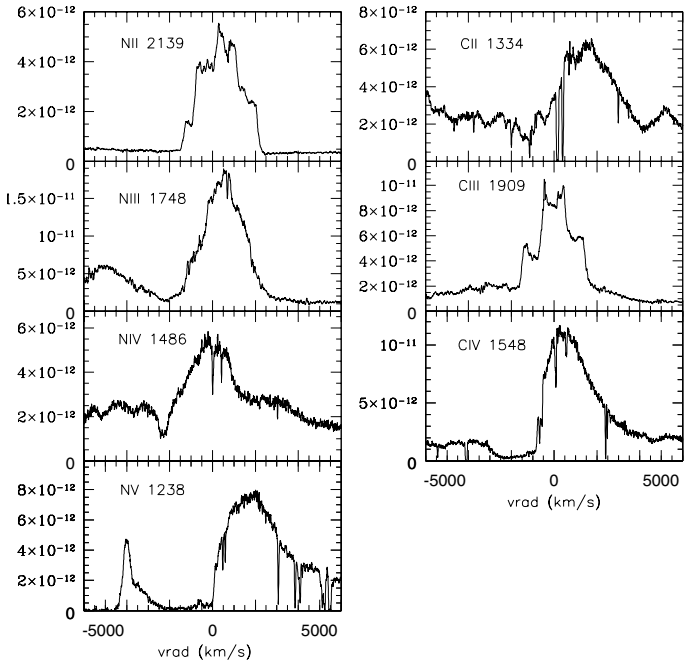

Fig. 15. Comparative profiles of the ultraviolet N^{+}-N^{+4} (*left*) and C^{+}-C^{+3} (*right*) resonance lines on day 105, see text for details. All fluxes are uncorrected absolute values, erg s^{-1} cm^{-2} Å^{-1}.

first noted in Paper II. In all cases, the emission was confined to the region within $1000 \leq |v_{\rm rad}| \leq 2000$ km s^{-1}. The N IV] 1486 Å and C III] 1909 Å lines had the same emission profile with no visible absorption. They differed in detail, the peaks being more marked in the C III] feature, but with essentially the same structure as the Balmer and other visible line at this epoch. The profiles were similar to He II 1640 Å and 4686 Å but with a stronger contrast between the central peak and the rest of the profile (see Paper II).

5.2. Resonance lines: ionization stratification in the ejecta

The ionization structure of the ejecta was traced by the comparison between the resonance lines of different ions at the same time. Examples for the especially complete set of ionization states available for C and N are shown in Figs. 15 (day 105) and 16 (day 173). Notice that the optical depth was low enough by day 173 that the full ejecta structure was in evidence and the profile variation in the UV resonance lines was similar to that seen in the optical lines. This is evidence that the line formation was principally by recombination. Instead, the day 105 sequence shows the effects of the large opacity of the ejecta at negative radial velocities on all but the intercombination lines. The asymmetries can be attributed to a combination of recombination of specific parts of the ejecta on the redward side and the residual effects of absorption on the blueward side. Our lack of coverage of the region longward of 1700 Å in the last three epochs precludes such detailed comparisons across the ionization states but we discuss the C IV and N V doublets at greater length below. Note, in particular, that there is an ion-dependent emission at around +2000 km s^{-1} on *all* the emission line profiles. On those lines formed from a single component, there is only one peak (e.g. C III] 1909 Å). For the doublets, the ratio of the emission strengths agrees with the ratio of the intrinsic line strengths.

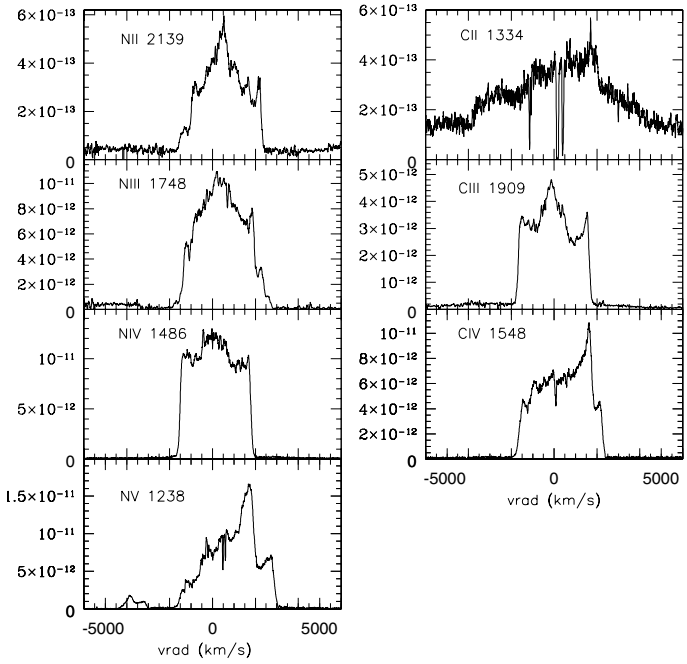

Fig. 16. Same as Fig. 15, for day 173.

5.3. Narrow absorption from resonance lines of low ionization state metals

Narrow absorption components, with *FWHM* ≈ 100 km s^{-1}, were observed on day 105 on most strong resonance transitions of neutral and singly ionized heavy elements; only those with low oscillator strengths were not detected. In Figs. 17 to 19 we display three epochs to show the evolution of these features. In general the lines displayed a single component at around

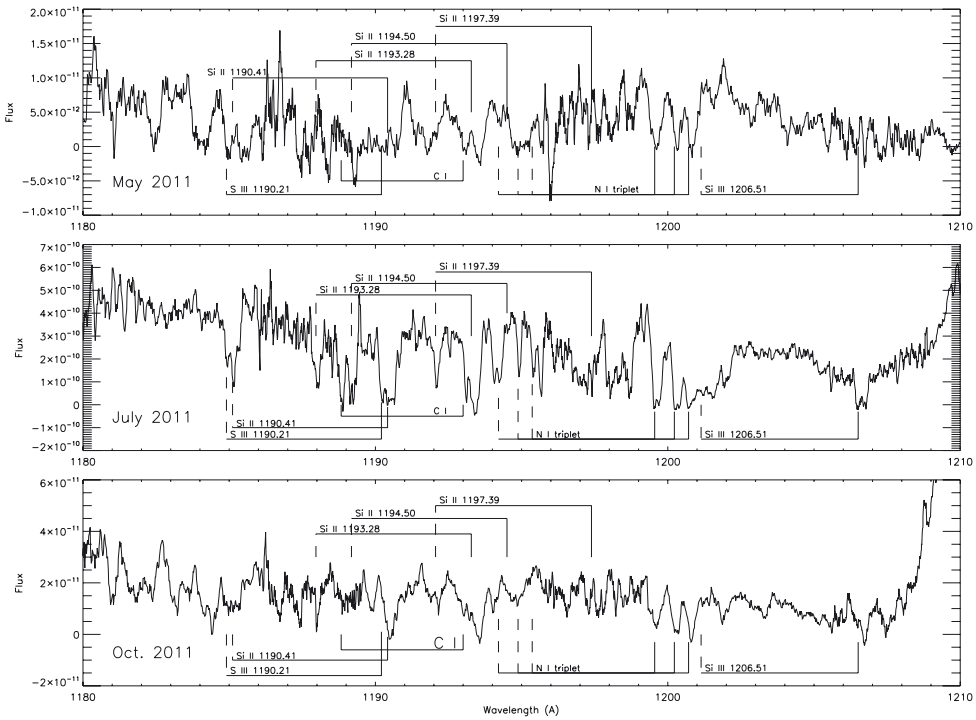

Fig. 17. Development of the wavelength range 1180–1210 Å during the first three epochs (*top to bottom*: days 23, 105, and 173). The high velocity (–1330 km s^{-1}) narrow absorption component is indicated with a link to the rest wavelength (in most cases the interstellar contribution). Note that narrow displaced absorption was also detected for transitions that did not display interstellar components, i.e., those from excited fine structure states. See text for details.

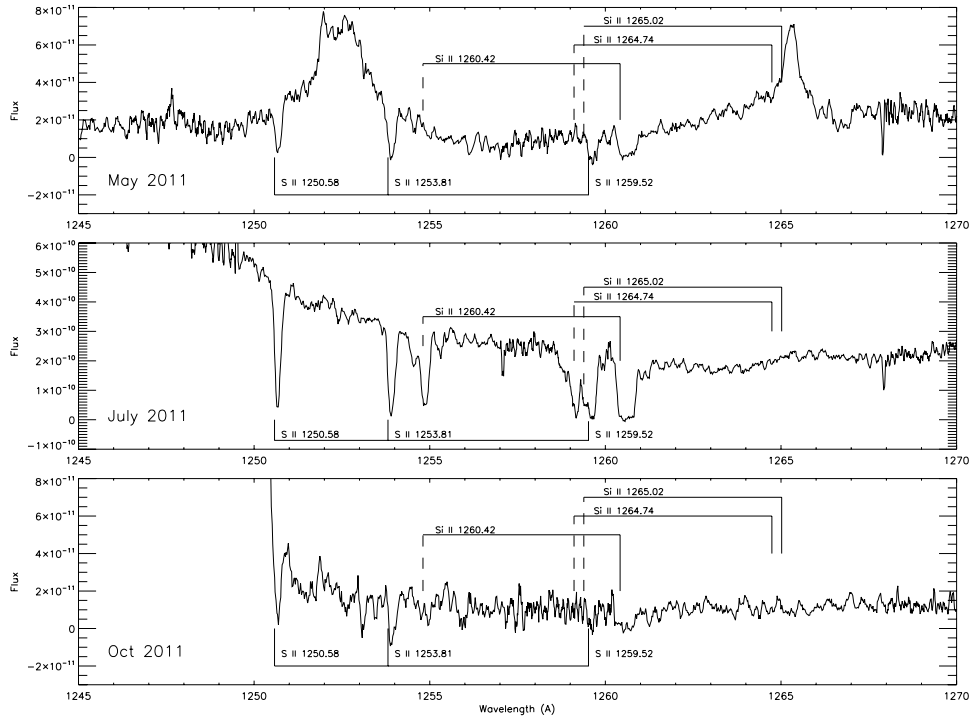

Fig. 18. Development of the wavelength range 1245–1270 Å as in Fig. 17.

–1300 km s^{-1}. Note that transitions without an interstellar counterpart from fine structure states with excitation energies below about 0.1 eV were also present among the high velocity narrow lines (e.g., Si II 1265 Å). In some cases, for instance Si II 1306 Å, there were accidental coincidences with either the high velocity and/or interstellar components of other transitions, such as O I 1304 Å. This complicated the interpretation but the changes in the nova spectrum relative to the ISM components, as noted above, helped in distinguishing the contributors. The column densities for the individual narrow line species measured on day 105 are listed in Table 5, the transitions from excited states are indicated by an asterisk. The composite curve of growth is shown in Fig. 20.

The relative abundance of Mg and S in the high velocity features is anomalous. The dominant ionization stage should be the same for these elements – that is, singly ionized – so the ratio of the column densities should be a good approximation of the abundance ratio of the elements. In a solar mixture, log Si/Mg = 0.09 ± 0.05 (Asplund et al. 2009). In contrast, the high velocity components have a log-ratio of $\approx -0.9 \pm 0.2$. This may be a fossil

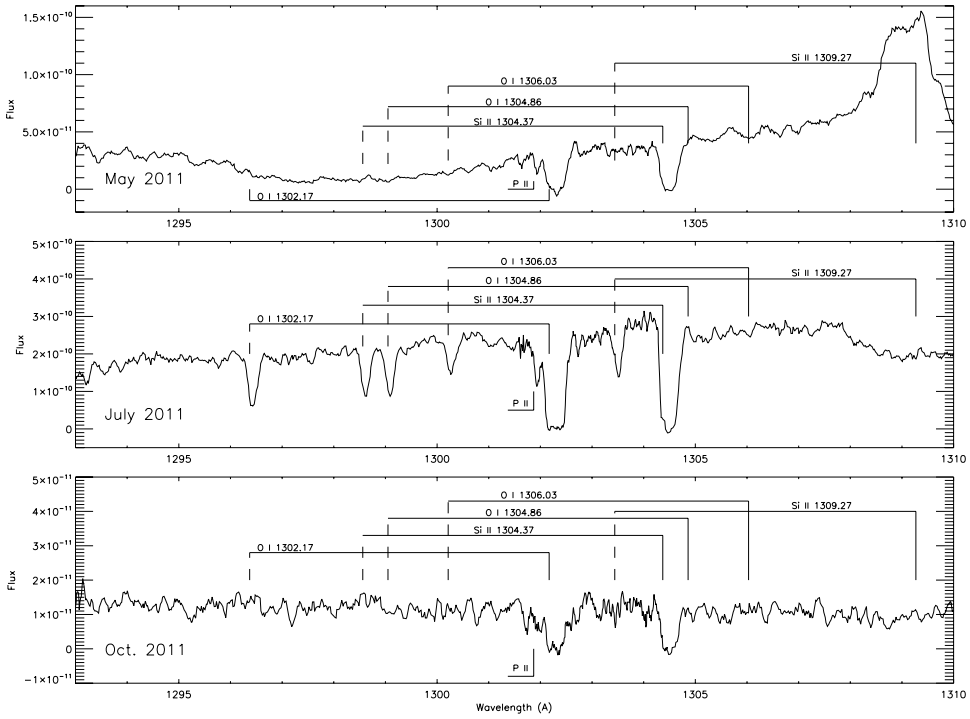

Fig. 19. Development of the wavelength range 1293–1310 Å as in Fig. 17.

Table 4. Equivalent widths (mÅ) for the high velocity narrow absorption features on day 105.

Species	Wavelength (vac, Å)	f-value	EW (mÅ)	V_{rad} range (km s^{-1})
Si II	1193.29	0.575	210 ± 40	–1390; –1260
Si II *	1194.50	0.737		–1380; –1260
Si II *	1197.39	0.150	165 ± 30	–1430; –1260
N I	1199.55	0.132		–1420; –1240
N I	1200.22	0.0869	105 ± 20	–1380; –1270
N I	1200.71	0.0432	111 ± 20	–1390; –1260
Si II	1260.42	1.22	320 ± 20	–1470; –1250
Si II *	1264.73	1.09	bl. S II 1259 Å (ISM)	–1470; –1280
O I	1302.17	0.0520	128 ± 15	–1380; –1270
Si II	1304.37	0.0928	92 ± 15	–1360; –1260
O I *	1304.86	0.0518	103 ± 20	–1360; –1280
O I **	1306.03	0.0519	90 ± 20	–1380; –1270
Si II *	1309.27	0.0800	86 ± 15	–1520; –1260
Si II	1526.71	0.133	185 ± 25	–1410; –1290
Si II *	1533.45	0.133	bl. Si II 1527 Å (ISM)	–
Al III	1854.72	0.557	682 ± 40	–1540; –1170
Al III	1862.79	0.227	bl. Al III 1854 Å (ISM)	–1480; –1170
Mg II	2796.35	0.608	231 ± 40	–1360; –1280
Mg II	2803.53	0.303	158 ± 50	–1370; –1280

Notes. Excited states are indicated by asterisks.

Table 5. Derived column densities (cm^{-2}) and range for the high velocity narrow absorption features on day 105.

Ion	Log N –1σ	Log N (cm^{-2})	Log N +1σ
Al III	15.35	15.65	15.98
Mg II	12.76	12.90	13.02
N I	14.15	14.27	14.38
O I	14.16	14.19	14.26
O I* (E = 0.019 eV)	14.03	14.12	14.20
O I** (E = 0.028 eV)	13.95	14.06	14.15
Si II	13.86	13.99	14.12
Si II* (E = 0.035 eV)	13.79	13.90	14.00

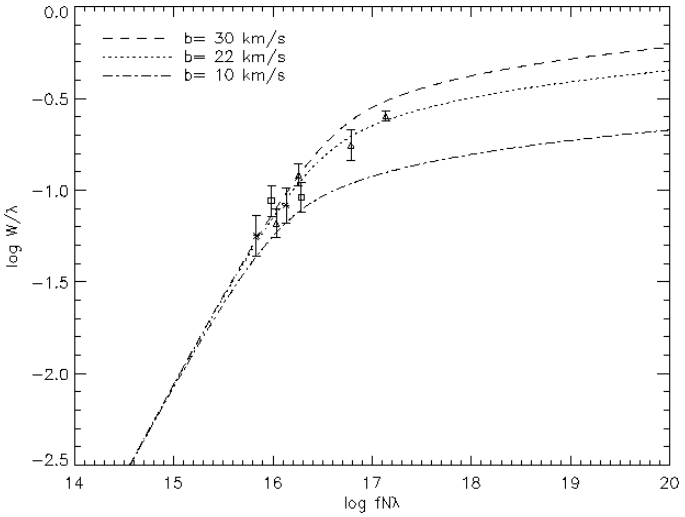

Fig. 20. Curve of growth for the narrow high velocity Si II absorption lines from the metallic ions on day 105 for Si II (triangles), Mg II (stars), and N I (squares) (see Tables 4 and 5 and text for details).

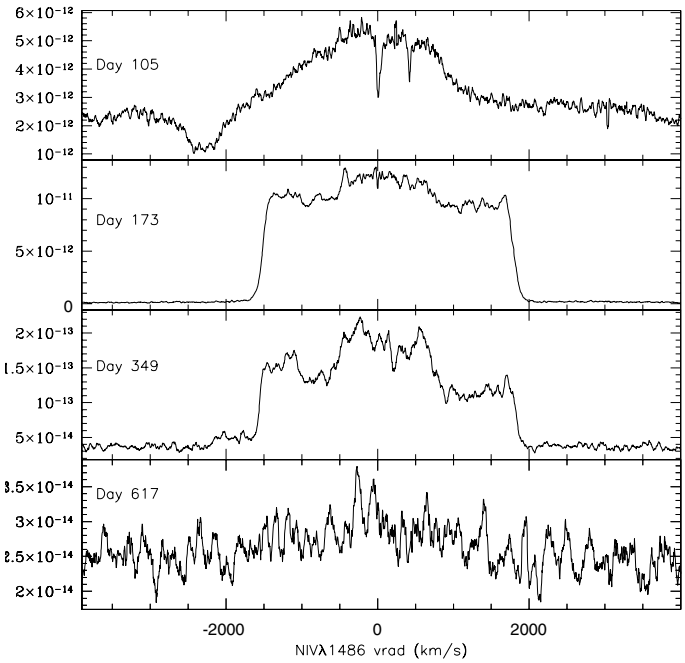

Fig. 21. The N IV] 1486 Å profile development. *From top to bottom*: day 105, day 173, day 349, day 617. Note the detached absorption line at feature at –2300 km s^{-1}.

of nucleosynthesis during the TNR but a ratio so different from unity is not currently predicted by nuclear-hydrodynamic models of CO novae (see e.g., Downen et al. 2013) and remains a challenge.

5.4. Detached P Cyg profiles on resonance and excited state transitions

In previous high resolution ultraviolet studies of novae after the end of the optically thick phase, the presence of P Cygni profiles with high velocity absorption troughs has been noted for the resonance lines (e.g. Shore et al. 1994, 2003; Cassatella et al. 2004). In the few cases where the observations have been unambiguous, after the disappearance of the overlying Fe-curtain lines, these have been seen on the C IV and N V lines and only in ONe novae (e.g. V1974 Cyg, V382 Vel at high resolution, LMC 1990 Nr. 1 at lower resolution). There was an indication of this in two recurrent novae (e.g. U Sco 1979 and LMC 1990 Nr. 2) but these were not well resolved. It therefore comes as a surprise that in the day 105 spectrum displayed a very strong *detached* P Cyg absorption extending to –2200 to –2000 km s^{-1} on N IV] 1486 Å resonance line, see Fig. 21. The maximum velocity was lower than the extreme on either the N V or C IV resonance doublets. By day 173 N IV] showed the same emission as the rest of the optically thin resonance lines.

The detection of detached, strong absorption features on UV lines that arise from *highly excited states* of C, N, and O has not previously been reported. The optical depth of the ejecta on day 105 appears to have still been sufficiently high that the lower levels of the iso-electronic transitions C III 2296 Å, N IV 1718 Å, and O V 1371 Å were sufficiently populated to produce absorption components as shown in Fig. 22. Their radial velocities were confined to the interval from –2200 to –1800 km s^{-1}, the same as N IV] 1486 Å resonance absorption and (roughly contemporaneously) the optical He I lines and He II 1640 Å, were not completely opaque although the absorption troughs on the C IV and N V P Cyg lines were. The N IV] 1718 Å – and C III 2296 Å lower states are populated by absorption from the ground state, 765 Å (UV1) and 977 Å (UV1), respectively. The

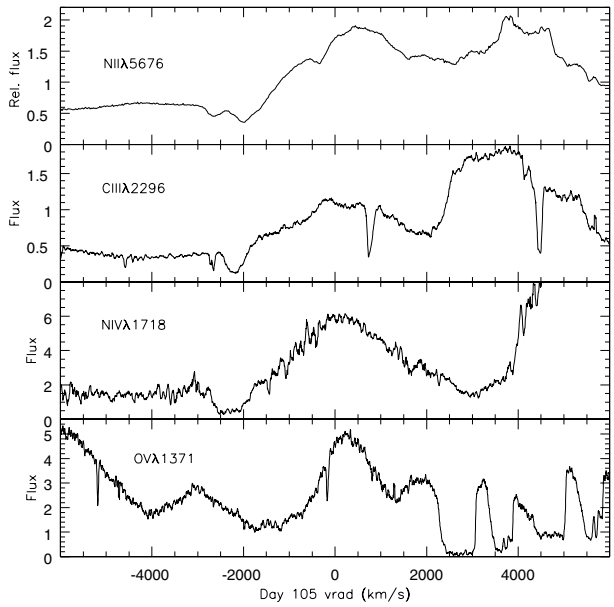

Fig. 22. P Cyg profiles for the excited state transitions from day 105; *from top*: N II 5676 Å (ESO day 73, shown for comparison), C III 2296 Å, N IV 1718 Å, O V 1371 Å. The feature on the C III profile at ≈+800 km s^{-1} is an artifact of the join between echelle orders. The absolute fluxes are scaled by 10^{-12} erg s^{-1} cm^{-2} Å^{-1}.

O V] 1371 Å line was detected with what may be a similar profile but the complexity of that portion of the spectrum precludes any quantitative analysis; its lower state is populated by 628 Å (UV1). We show the partial Grotrian diagram for these ions in Fig. 24. The absorption was displaced to higher velocities than those observed during optical maximum on any transitions and compatible with the blueward extension of the C IV and N V absorption troughs. These discrete absorptions had disappeared by day 173. We show the He I 5875 Å line development as a

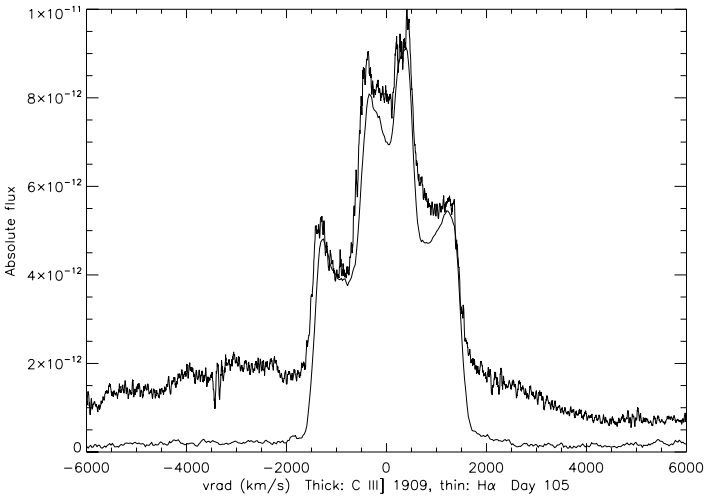

Fig. 23. Comparison of C III] 1909 Å (thick) and Hα (thin) for day 105, both from STIS spectra.

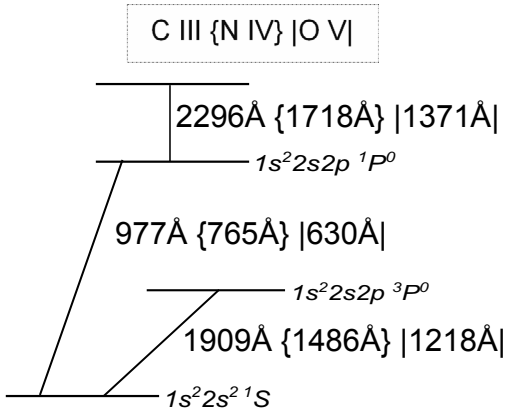

Fig. 24. Sample Grotrian diagram of the isoelectronic transitions of C^{+2}, N^{+3}, and O^{+4} that display detached absorption trough P Cyg profiles during the transition stage. The resonance lines are also indicated and the FUV exciting transitions. See text for details.

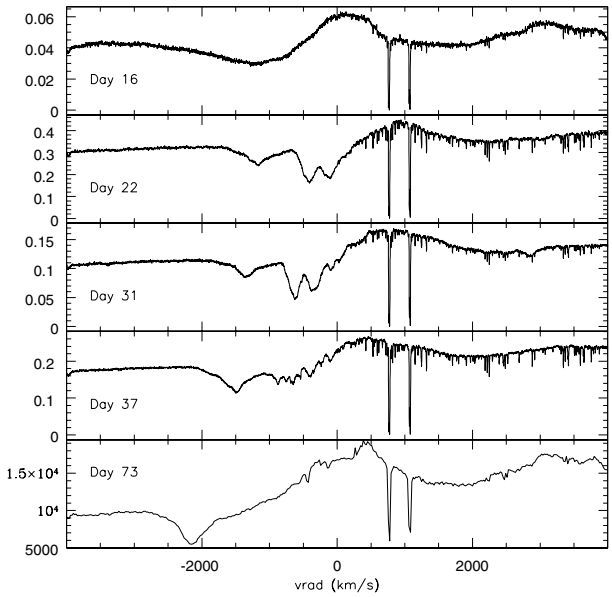

Fig. 25. Time development of the high velocity absorption on He I 5876 Å line for dates (*from top*): 2011 Apr. 14, Apr. 23, May 15, Jun. 26.

comparison with the excited state profiles in Fig. 25. The velocities are the same as those seen on the UV profiles, and from the same structures, excited as the ionization wave progressed outward through the ejecta. This suggests that the appearance of these absorption components was not an extraordinary phenomenon peculiar to T Pyx but simply that the UV spectra were, by chance, obtained at the right moment.

Since these detached absorption features covered a restricted velocity interval, this implies that the FUV was not completely optically thick throughout the ejecta but that specific parts were. The "tuning process" left the bulk of the emission, formed by recombination, transparent while the absorption was produced along the line of sight to the underlying WD. This also indicates that there was a strong far ultraviolet source already present but still optically thick in the resonance line shortward of 1000 Å. For He II this extends the range to 303 Å, based on the He II 1640 Å line profile. The absorption components were absent for intrinsically weak transitions. For instance, for the iso-electronic resonance lines N IV] 1486 Å and C III] 1909 Å, here was no detectable absorption on C III]. It showed, instead, the same profile as Hα, see Fig. 23.

6. Discussion

A benefit of the ultraviolet portion of the spectrum is the number of ionization states available for C (C^{+} to C^{+3}, N (N^{0} to N^{+4}), and O (O^{0} to O^{+4}). In particular, for days 105 and 173 the iso-electronic sequence C III, N IV, and O V was complete for both resonance lines and the excited states and it was possible to study the ionization structure of the ejecta and its history throughout the X-ray phase.

6.1. Ionization structure of the ejecta derived from the carbon, nitrogen, and oxygen sequences

An examination of the sequence of profiles passing from the singly to four times ionized nitrogen, and singly to triply ionized carbon, indicate that the individual emission peaks were due to differential recombination in the ejecta. The peak at +2000 km s^{-1} was seen in both components of the C IV 1548, 1550 Å and the N V 1238, 1242 Å doublets but can be traced through three ionization stages. The higher the ionization stage, the stronger the feature. The blueshifted portion of the profiles were systematically weaker than the redward side, indicating that the transition was still marginally optically thick and that the ionization was not yet complete for the ejecta beyond C^{+3} and N^{+4}. The lack of absorption was likely due to the emission line cutoff, it was not visible on the N V 1238 Å or C IV 1548 Å component while it *was* seen on the other member of the doublet against the combined emission. In other words, the ejecta were optically thick in the respective ions at high velocity – hence larger radius – while the inner, denser portions of the ejecta were not as ionized. It is significant that for the day 173 observation, that was at the peak of the X-ray emission observed with *Swift*, all of the optical emission lines had essentially the same profiles and covered the same velocity interval as the resonance lines of the lower ions observed in the UV (as in Fig. 23 for C III] versus Hα, see also Paper II).

The enhanced emission between $+1400 \leq v_{\rm rad} \leq +1900$ km s^{-1} on both components of the C IV and N V doublets can be explained as enhanced recombination in the receding

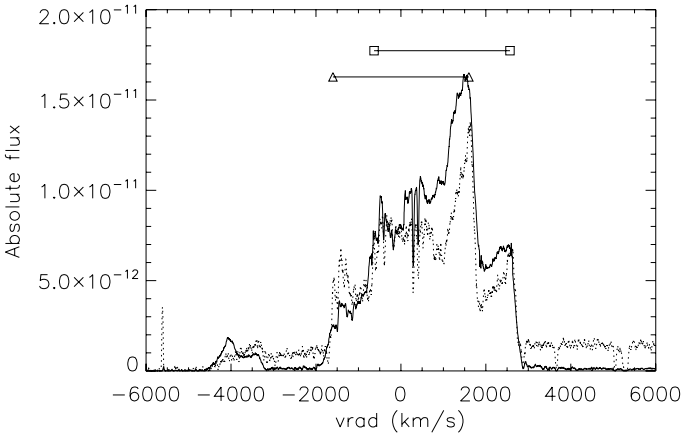

Fig. 26. Recombination of N V 1238, 1242 Å on days 173 (solid) and 348 (dot, scaled by a factor of 20 in flux). The blueshifted and redshifted velocities of the emission peaks are shown for the two doublet components as described in the text.

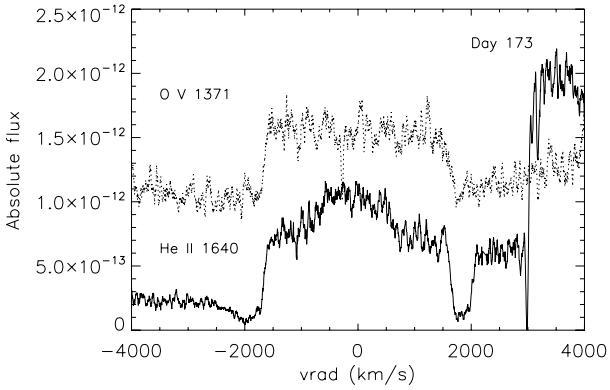

Fig. 27. The He II 1640 Å and O V 1371 Å line profiles on day 173, illustrating how different ions probe different ejecta structures.

parts of the ejecta. We show in Fig. 26 the details for the two components of the N V doublet, compare this with the C IV doublet shown in Fig. 16, above. The excess emission corresponds to the same absolute value of radial velocity as the absorptions but with a different structure. Since the emission was from the whole receding ejecta while the absorption (see below) was only produced along a single line of sight toward the WD, the profiles should be different. The emission was always strongest on the highest ionization stage and this is consistent with recombination that continued after the XR turnoff.

Another view of the ionization structure is provided by a comparison between the O V 1371 Å and He II 1640 Å profiles, on day 173 when both were only in emission (Fig. 27). The He^{+} was more peaked toward the inner ejecta than in the O^{+4}. This would be expected when the freeze-out phase occurs, the higher ionization should be predominantly at the lowest densities with the lowest ionization stage being determined by the maximum recombination rate in the inner parts of the ejecta.

In Paper II we derived the electron density, n_e and temperature T_e in the ejecta for days 173 and 348 using the optical [N II] and [O III] multiplets. For the second date, having both diagnostics, we found $T_e \approx 3.9 \times 10^4$ K and for the inner portion of the ejecta $n_e \approx 5.4 \times 10^5$ cm^{-3}. Since the later date was after the end of the XR emission, recombination should be dominated by the rate of expansion. Then taking a time interval of ≈170 days after the end of the photoionization era, the electron density of

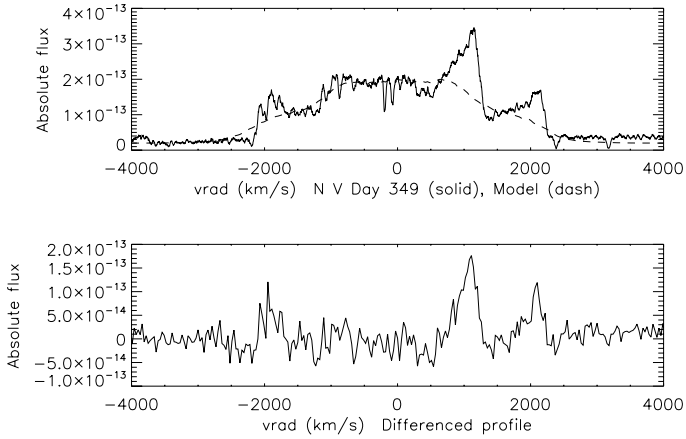

Fig. 28. *Top*: recombination components on N V 1238, 1242 Å on for day 349 (solid) compared with a bipolar cone model (see text for description). *Bottom*: differenced profile.

that part of the ejecta whose ionization is "frozen" can be derived. Using the recombination coefficients from Pequignot et al. (1991) for C^{+3} and N^{+4} we obtain $n_{e,\star} \approx 3 \times 10^4$ cm^{-3}. This is the density in the ejecta at that location where the recombination rate balances the expansion since the electron density at any radius varies as t^{-3}. From this, the radius corresponding to $n_{e,\star}$ is about $2.7R_{in}$, where R_{in} is the inner radius, in thee spectra at 100 km s^{-1}. But since this is ballistic expansion, the ratio is the same as that of the expansion velocities so with a minimum $v_{rad} \approx 1000$ km s^{-1} this corresponds to about 2700 km s^{-1}. For a lower n_e and later times, for instance at day 617, this radius displaces inward, consistent with the velocities of the absorption lines in the last spectra. The discreteness of the profiles is not, however, explicable with only a single radius of recombination since the same structures were visible throughout the expansion. There must be specific density enhancements at certain radii that produce the multiple components. To obtain a clearer view of the emission features, we used a bipolar ejecta model of the sort described in Paper II. We assumed the same maximum outward velocity, $v_{rad,max} = 4000$ km s^{-1}, inner angle of 7°, outer angle of 35°, ejecta thickness $\Delta R/R = 0.5$, and inclination $i = 20°$ as derived from modeling the optical emission line profiles. The model profile combined two profiles of equal transition strength at the rest wavelength of each doublet component and scaled in flux to match the zero radial velocity peak and subtracted from the observation. The model N V profile and extracted emission components are displayed in Fig. 28[2].

6.2. Absorption lines from the ejecta during the post-outburst stage, days 617 and 834

The spectrum from day 617 seems to hold the final key to the ejecta structure. The He II 1640 Å line was dominated by the core emission which had weakened since day 349, and the wings – if present – were too faint to be seen above the noise. N IV] 1486 Å and S IV 1400 Å were not detected. The C IV 1550 Å doublet was weakly in emission in the velocity range around ±1000 km s^{-1}. Far more important, however, were the narrow absorption lines observed at –1700 km s^{-1} and –1300 km s^{-1} on *both* – and only in – the N V and C IV doublets (Fig. 29). These

[2] Note that our bipolar cone models do not include discrete structures, hence any departure of the profile from symmetry is made more evident by the comparison.

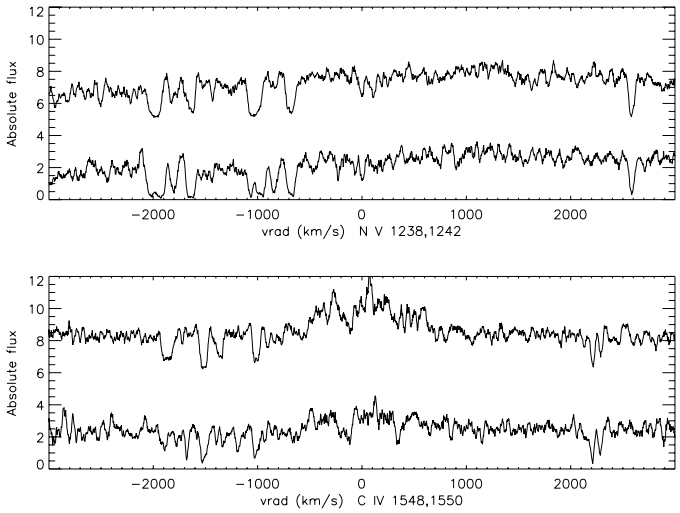

Fig. 29. Comparison of the N V 1238, 1242 Å and C IV 1548, 1550 Å absorption features in the last STIS spectra. In *each panel* we show day 617, shifted upward for clarity, and day 834 (*lower*), all fluxes are scaled to 10^{-14} erg s^{-1} cm^{-2} Å^{-1}. The doublet centroid was chosen as the reference wavelength in each case for displaying the changes. See Fig. 30 for a detailed view of NV in the two epochs.

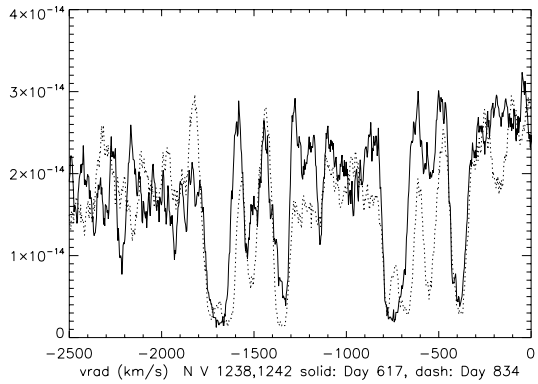

Fig. 30. Detailed view of the N V 1238, 1242 Å absorption features from day 617 (solid) and day 834 (dot).

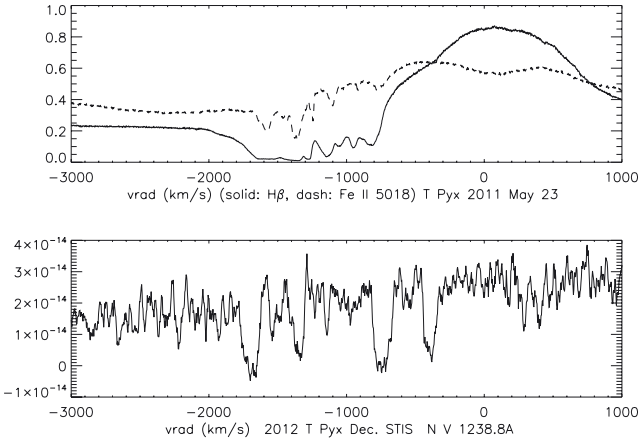

Fig. 31. Comparison of early optical spectral line profiles (day 33, Hβ and Fe II 5018 Å) near maximum optical brightness with the day 617 STIS spectrum at N V 1238, 1242 Å absorption lines. As for Si IV, there was a component at –1300 km s^{-1} but there is no corresponding absorption at the higher velocity Si IV feature.

had similar velocity widths, about 200 km s^{-1}. For a ballistic velocity law, this corresponds to a thickness $\Delta R/R(t) \approx 0.15$ for each of the two components. Only two components were present (see Fig. 30).

Compared with the complexity of the earlier spectra (see Fig. 31), especially the rather narrow velocity range covered by these last absorption features, this may seem odd. However, recall that in the earlier stages there was still a substantial optical depth in the ejecta and the pseudo-photosphere in the ultraviolet was still subtending a large solid angle. The emission portion of the extended P Cyg profiles also increased the surface against which the ejecta could absorb, hence components were detected at very low velocities on the optical line profiles since the absorption from the ejecta was against an extended source. By day 617, long after the end of the XR emission and the transition to complete transparency in the ejecta, the line of sight toward the central WD was a pencil beam. It passed through only two structures whose widths were consistent with the narrowest features seen during the optical absorption line stages near visual maximum light, long before the thinning of the UV or FUV. These must be individual filaments, not the boundary of the bipolar ejecta, and they were consistently present throughout the event since the N V and C IV components correspond to absorption lines seen on the Balmer and other lines early on. These late time spectra, after the end of the WD X-ray illumination, showed the freeze-out stage, when the recombination of the ejecta is impeded by the expansion rate and the decrease in the local number density (see, e.g. Shore et al. 1996; Vanlandingham et al. 2001).

The last spectrum, on day 834, supports and extends these conclusions. It showed distinct changes in the C IV and N V absorption lines (Fig. 29). A third feature, at –1500 km s^{-1}, that had been weakly present on day 617 increased from 135 mÅ to 193 mÅ for the 1238 Å component and from 30 mÅ to 210 mÅ for the 1242 Å doublet component with an uncertainty of 10% determined from measuring the interstellar O I 1302, 1304 Å lines. The main absorption feature at –1700 km s^{-1} had separated into two weaker components at –1735 and –1650 km s^{-1}. The CIV 1550 Å doublet absorptions were much weaker but still present. This indicates an increase in the ionization of the outer portions while the inner region was still weakly recombining. The velocities of the features remained invariant. There was no detectable emission on N V, and that on both C IV and He II 1640 Å had decreased by about a factor of 2 from day 617 with no detectable change in the line width or profile. The only other absorption lines were interstellar including Lyα.

The clearest view of the ejecta structure emerges from a comparison with the day 105 spectrum. For instance, on day 105 the O I 1302, 1304 Å showed multiple components, like the Na I D lines at an earlier stage but were considerably narrower. While the Na° absorptions spanned ≈300 km s^{-1} on day 33, the O I lines were about a factor of 3 narrower in velocity (FWZI). The same was true for the high ionization lines at later epochs. On day 617 relative to the span of the Si IV doublet components on day 105. The velocities were similar, to within about 30%, independent of epoch, but the maximum radial velocity was *always* higher in the UV lines by as much as a factor of 2. An important result is that the narrow lines observed on day 105 for the heavy metal low ionization transitions, coincided with *one* of the components on the C^{+3} and N^{+4} on days 617 and 834, the component at ≈–1400 km s^{-1}. The same was displayed by the Si^{+3} absorption components on day 105. But in all cases for the higher ionization species there was also a more extended

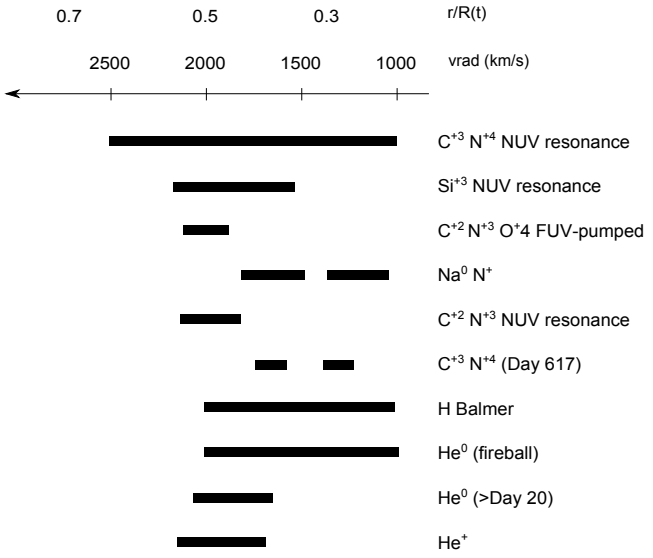

Fig. 32. Schematic ionization-dependent velocity structure. The ionic species are indicated, the velocity range is transformed into radial distance using a ballistic ejection and a maximum velocity of 4000 km s^{-1}.

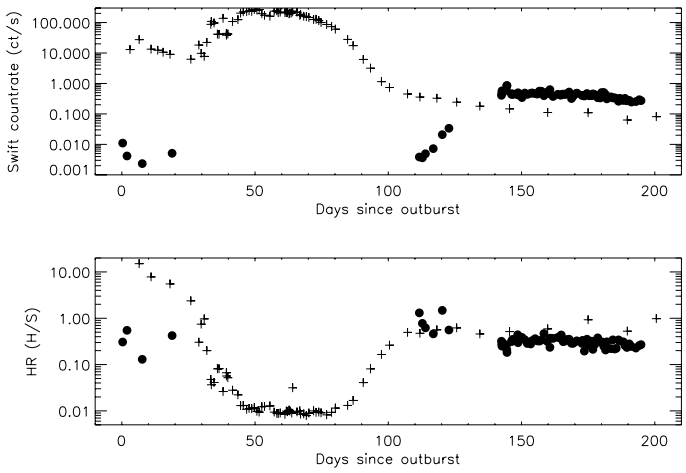

Fig. 33. *Top*: comparative *Swift*/XRT light curves of RS Oph 2006 (cross) and T Pyx 2011 (dot) until day 200 after outburst for both. *Bottom*: hardness ratio showing that the supersoft phase was not seen for the T Pyx observations, the optical depth in the soft XRs completely obscured the white dwarf (see text for discussion). The H/S ratio for T Pyx used (0.8–10 keV)/(0.3–0.8 keV). For RS Oph we used the data in Schwarz et al. (2011) with the H/S ratio defined by (1–10 keV)/(0.3–1 keV).

range for the absorption features beyond the limit of anything detected for the lower ionization species. A schematic of the derived structure of the ejecta on this date is shown in Fig. 32. All ions, regardless of the stage, systematically showed the lower velocity absorption. The higher velocity components were seen only on the highest ions, weighted by the abundance of the tracing species. We note that the same features were also seen in the Fe II lines during the early stage of the outburst (Paper I, see Fig. 31).

The coincidence of the recombination emission and absorption lines in the two sides of the ejecta relative to the WD cannot be mere chance. Something must be imposing this structure on the matter at the initial explosion and ejection. The structures we infer are not mere threads or knots. They cover considerable portions of the bipolar lobes. These are density enhancements, not *only* temporary markers of the ionization and recombination fronts as they move through the ejecta. Their velocity widths are constant even when they disintegrate into smaller knots (as seen in the optical spectra). When seen against the P Cyg emission components in line profiles, their velocities can reach almost to the escape velocity fro the WD, this also implies a substantial lateral extent. Had T Pyx been oriented differently, however, we would have seen a very different picture (e.g., Shore 2013).

6.3. The X-ray emission

Although we have used the phrase "supersoft source (SSS) phase" to describe the XR emission there is an alternative interpretation that may make sense for the high energy emission of T Pyx, illustrated in Fig. 33. The WD in the symbiotic-like recurrent nova RS Oph was extensively observed during the 2006 event by *Swift* and *Chandra* (see e.g. Ness et al. 2009; Osborne et al. 2011; Schwarz et al. 2011). The source went through a marked SSS phase after the ejecta had essentially broken out of the wind and the shock was not the primary emitter. However the source revealed itself, the phase from about 50 to 200 days was marked by an overwhelmingly soft XR emission with all of the associated signatures of the SSS. A rapid turnoff time in T Pyx, similar to that observed in RS Oph, is consistent with a massive WD as implied from the large luminosity calculation from the Fe-curtain stage. If the observed *Swift* light curve and HR evolution in T Pyx is just the cooling WD after the SSS phase then the Fig. 33 sets an upper turnoff limit, $t_{\rm off}$, of about about 140 days. So *if* the WD in T Pyx went through a similar development following the explosion, the XRs detected by *Swift* after day 100 may *not* have been a SSS at all but the hot ejecta now becoming optically thin due to the expansion. Alternatively, Tofflemire et al. (2011) reported the *Chandra* observation of a soft source spectrum on day 200 so the late time emission may well have included a SSS. The presence of a source, hidden from the external observer by the opaque layers and the high inferred interstellar column density, is supported by the observations we described on day 105 (Sect. 5.4) that indicate an ionization of the ejecta consistent with a source having a temperature of about 50 eV. At no time after first visibility did the hardness ratio detected with *Swift* fall far below unity, the requirement for the SSS identification. Instead, it remained near unity for the whole time until turnoff, like RS Oph. For photons at 0.5 keV, in the middle of the soft *Swift* XRT band, a neutral hydrogen column density $N_{\rm H} \approx 1.2 \times 10^{22}$ cm^{-2} suffices to produce an optical depth of about 10 that would reduce the count rate for a SSS by a factor of 10^5 while those at 3 keV would have an optical depth of about 5, consistent with the results shown in Fig. 33 (and see also Kuulkers et al. 2011). This $N_{\rm H}$ is about a factor of 10 greater than the interstellar value derived in Paper II based on extinction, the Lyα line profile, and 21 cm measurements (see Sects. 3 and 4.5, above)[3].

[3] The mass of the ejecta corresponding to this column density can be estimated assuming that the outer radius of the ejecta on day 50 was $R = 1.5 \times 10^{15}$ cm for a maximum expansion velocity of 4000 km s^{-1}. The inner electron density was $n_{\rm e,0} \approx 5 \times 10^7$ cm^{-3}. Scaling the density derived for day 173 assuming an inverse cube scaling with time for the number density predicts $2.7 \times 10^8 n \leq n_{\rm e,0} \leq 1.2 \times 10^9$ cm^{-3}, suggesting that the $n({\rm H}^\circ)/n({\rm H}) \approx 0.1$ on day 50. With the bipolar geometry, fractional ejecta thickness $\Delta R/R = 0.7$, and filling factor $f = 0.03$ derived in Paper II, the mass inferred from this column density is $\approx 4 \times 10^{-6}\ M_\odot$, with an estimated uncertainty of about a factor of two.

6.4. Final points

An important analogy between our findings and other areas of astrophysics is found in the cosmological re-ionization epoch and the evolution of the Lyα forest. In the T Pyx ejecta, the ionization source – the hard emission from the WD – had a finite lifetime and the recombination wave of the first stage following the initial fireball was replaced by an ionization wave. This front, in turn, was inhibited by the expansion so the outer ejecta remained highly ionized while only the inner, lower velocity and higher density, portions could partially neutralize. In other words, what we witnessed here is a generic behavior characteristic of expanding media. The same reasoning applies to the interpretation of the centimeter radio emission that Nelson et al. (2012) have interpreted as a late-stage wind from the system. The ejecta, being neutral in the early expansion stages, were also radio silent. On re-ionization, however, the standard theory applies and the progressive decrease of the optical depth as a function of frequency then reproduces the flux variations in different bands. The cosmological analogy is, therefore, physically consistent and much more than a mere metaphor. It highlights the fact that the phenomenology we observed in this recurrent *cannot* be explained by a wind. In a continuous outflow, any density feature must advect in the wind and, therefore, displace in velocity and strengthen. It cannot break up into filaments of absorption nor remain stationary over thousands of traversal times for the matter. Were the absorption features we and others have observed in nova outburst spectra the result of discrete absorption components (DACs) in a steady wind, the lines would show saturation effects due to the terminal velocity of the flow. We do not see that and, indeed, the structures that were detected in one ionization stage at some epoch are traceable in others of later stages. The P Cyg troughs are not consistent with a velocity saturation effect such as would be expected from (and seen in) the ionized winds of massive stars. Since the phenomena we have described are seen also in sparser data sets for other novae of all types, our results call the question regarding the origin of the bipolarity and the fragmentation/shell structures.

7. Conclusions

The stationarity of the narrow absorption features, and their optical depth variations, are *inconsistent* with a wind during any of the phases we observed. The detection of recombination events *in emission* at the same outward velocities (relative to the WD) during the post-XR era in the earlier absorption line profiles supports this view. The changes in the ionization of the ejecta revealed from the absorption lines also was consistent with expansion-limited recombination from ballistic freely expanding ejecta. The onset of the re-ionization wave coincided with the rise of the centimeter radio and its subsequent evolution was also what is expected from ejecta. The geometry inferred from the ultraviolet emission line profiles is the same as we had previously obtained from the optical spectra alone once the matter became transparent. The detached absorption features on the excited state C, N, and O lines was exactly analogous to what was observed on the optical Fe-peak lines, the pumping by resonance transitions arising at the same outward velocities within the ejecta. In summary, the sequence of profiles and the overall spectral evolution of T Pyx during this outburst, which was not exceptional among those previously observed, demonstrate the explosive ejection of the envelope during this event and that there is no need to invoke super-Eddington winds or any continuous outflow.

Acknowledgements. We thank our colleagues Jan-Uwe Ness, Bran Warner, Kim Page, Julian Osborne, Luca Izzo, Jordi José, Massimo Della Valle, Tim O'Brien, Bob Williams, and Fred Walter for vigorous, insightful, and deep exchanges, and the (anonymous) referee for a close reading and very helpful guidance. We thank Alessandro Ederoclite for discussions and correspondence regarding the ESO spectra. The HST observations were performed on GO-12200 (Schwarz, PI) and DDT-12799 and GO-12890 (Sion, PI). Support for program #12200 was provided by NASA through a grant from the Space Telescope Science Institute, which is operated by the Association of Universities for Research in Astronomy, Inc., under NASA contract NAS 5-26555. We thank the STScI director, Matt Mountain, for a generous allocation of Director's Discretionary time to observe T Pyx in its late stages and Neil Gehrels for massive allocations of *Swift* observing time. SNS warmly thanks Patrick Woudt for an invitation to the University of Cape Town and Petr Harmanec for a visiting position at the Charles University (Prague) and Daniela Korcakova for many valuable discussions. S.S. acknowledges partial support form NSF and NASA grants to ASU.

References

Asplund, M., Grevesse, N., Sauval, A. J., & Scott, P. 2009, ARA&A, 47, 481
Bode, M. F., & Evans, A. 2008, Classical Novae, 2nd edn. (Cambridge University Press)
Cardelli, J., Clayton, G., & Mathis, J. 1989, ApJ, 345, 245
Cassatella, A., Lamers, H. J. G. L. M., Rossi, C., Altamore, A., & González-Riestra, R. 2004, A&A, 420, 571
Chesneau, O., Meilland, A., Banerjee, D. P. K., et al. 2011, A&A, 534, L11
Downen, L. N., Iliadis, C., José, J., & Starrfield, S. 2013, ApJ, 762, 105
Gilmozzi, R., & Selvelli, P. 2007, A&A, 461, 593
Howk, J. C., Sembach, K. R., & Savage, B. D. 2006, ApJ, 637, 333
Jenkins, E. B. 1986, ApJ, 304, 739
Jenkins, E. B. 2009, ApJ, 700, 1299
Jenkins, E. B., & Tripp, T. M. 2006, ApJ, 637, 548
Kalberla, P. M. W., McClure-Griffiths, N. M., Pisano, et al. 2010, A&A, 512, A14
Kuulkers, E., Orio, M., Osborne, J. P., et al. 2011, ATel, 3647
Morton, D. C. 1991, ApJS, 77, 119
Nelson, T., Chomiuk, L., Roy, N., et al. 2012, ApJ, submitted [arXiv:1211.3112]
Ness, J.-U., Drake, J. J., Starrfield, S., et al. 2009, AJ, 137, 3414
Osborne, J. P., Page, K. L., Beardmore, A. P., et al. 2011, ApJ, 727, 124
Payne-Gaposchkin, C. H. 1957, The Galactic Novae (North-Holland Pub. Co.)
Pequingnot, D., Petijean, P., & Boisson, C. 1991, A&A, 251, 680
Savage, B. D., & Sembach, K. R. 1986, ARA&A, 34, 279
Schaefer, B. E., Landolt, A. U., Linnolt, M., et al. 2013, ApJ, 773, 55
Schwarz, G. J., Shore, S. N., Starrfield, S., et al. 2001, MNRAS, 320, 103
Schwarz, G. J., Ness, J.-U., Osborne, J. P., et al. 2011, ApJS, 197, 31
Selvelli, P., Cassatella, A., Gilmozzi, R., & González-Riestra, R. 2008, A&A, 492, 787
Sembach, K. R., & Savage, B. D. 1992, ApJS, 83, 147
Shore, S. N. 2013, A&A, 559, L7
Shore, S. N., Augusteijn, T., Ederoclite, A., & Uthas, H. 2011, A&A, 533, L8 (Paper I)
Shore, S. N., Schwarz, G. J., De Gennaro Aquino, I., et al. 2013a, A&A, 549, A140 (Paper II)
Shore, S. N., De Gennaro Aquino, I., Schwarz, G. J., et al. 2013b, A&A, 553, A123
Tofflemire, B., Orio, M., Kuulkers, E., et al. 2011, ATel 3762
Uthas, H., Knigge, C., & Steeghs, D. 2010, MNRAS, 409, 237
Welty, D. E., & Fowler, J. R. 1992, ApJ, 393, 193